Composite Structures 299 (2022) 116043

Contents lists available at ScienceDirect

Composite Structures

journal homepage: www.elsevier.com/locate/compstruct

Review

Damage monitoring methods for fiber-reinforced polymer joints: A review

Wencai Li, Genevieve Palardy *

Department of Mechanical and Industrial Engineering, Louisiana State University, 3261 Patrick F. Taylor Hall, Baton Rouge, LA 70803, United States

ARTICLE INFO

Keywords:
Structural health monitoring
Fiber-reinforced polymers
Joints/joining

ABSTRACT

As the application of composite materials in structural parts continues to increase, so does the importance to monitor the structure's health condition during their entire service life. This paper presents a comprehensive review on damage monitoring methods focusing on fiber-reinforced polymer joints: adhesively bonded, mechanically fastened, and welded. In this review, structural health monitoring (SHM) methods are classified into two major groups: intrinsic sensing (embedded at the bond line) and extrinsic sensing (placed outside the interface). Main intrinsic techniques include fiber optic sensors, piezoelectric sensors (e.g., electromechanical impedance), and nanocomposite-based monitoring. The latter has attracted significant interest in the past years and is emphasized from its applications for different joining methods. For extrinsic sensing, several non-destructive testing techniques are considered to evaluate the integrity of composite joints, including acoustic emission, acousto-ultrasonic wave (e.g., guided wave), structural vibrations and acoustics, laser shock adhesion test, electromechanical impedance (e.g., piezoelectric sensors), and ultrasonic non-destructive testing (NDT). For each sensing method, damage monitoring is discussed from three aspects: i) damage type, ii) damage location, and iii) damage severity. Novel methods, significant results, current trends, and challenges are summarized. Finally, further research efforts needed in this field are recommended.

1. Introduction

The past few decades have witnessed the sustained growth of composite materials' applications due to their light weight, high corrosion resistance, excellent mechanical properties, and capability to be shaped into complex geometries, making them promising metal substitutes [1–7]. Nowadays, an increasing number of large or integrated structural components in aerospace, automotive, energy, civil engineering, and marine industries are made of composite materials, in which assembly technologies are usually required. Consequently, the rapid growth in the use of composite materials has resulted in a growing interest and need for reliable joining techniques.

Joining is an important step in the manufacturing of large and complex composite structures. To date, widely used joining techniques for composite materials can be divided into three major categories: mechanical fastening, adhesive bonding, and fusion bonding (welding). Mechanical fasteners come in many forms, such as bolts, rivets, screws, anchors, and inserts, providing several advantages, such as ease of quality control, disassembly, and repair [8]. However, on the other hand, mechanical fasteners are usually vulnerable to galvanic corrosion and lead to increased composite weight, stress concentrations, and failures [9,10]. For this reason, over the past decades, adhesive bonding for composite structures has attracted attention and been extensively explored in the literature [11–26]. Compared to mechanical fasteners, adhesively bonded joints overcome some disadvantages and offer additional advantages: i) eliminating mechanical elements may lower overall weight and cost, ii) suitable to join dissimilar materials, and iii) providing more uniform stress distribution, better damage tolerance and corrosion resistance, while maintaining the adherends' structural integrity and providing a smoother appearance [20,26]. Despite the advantages of adhesive bonding, there are still some drawbacks, for example, rigorous surface preparation requirements, long curing time, sensitive to environmental factors like temperature and humidity, and not suitable to bond all thermoplastic matrices [10,18,21].

The third joining category, fusion bonding (welding), has shown possibility as an alternative to conventional techniques (e.g., mechanical fastening and adhesive bonding). It is traditionally employed for unreinforced and reinforced thermoplastics, but also has potential for vitrimers, recyclable thermosets, liquid thermoplastics, and dissimilar materials [27–30]. Fusion bonding occurs via melting of the joint interface, while being heated above the matrix' glass transition temperature or melting temperature, and then consolidating under pressure

* Corresponding author.
E-mail address: gpalardy@lsu.edu (G. Palardy).

https://doi.org/10.1016/j.compstruct.2022.116043
Received 1 February 2022; Received in revised form 1 July 2022; Accepted 4 August 2022
Available online 8 August 2022

when cooling down [10,31]. Like adhesive bonding, welding addresses some of the inadequacies of mechanical fastening, eliminating stress concentrations introduced by holes, as well as potentially reducing processing time and manufacturing cost. Additionally, in contrast with adhesively bonded joints, fusion bonding does not need long curing times or vigorous surface preparation. Inevitably, some disadvantages include: i) nonuniform heat distribution, ii) limited joint complexity for some welding techniques, and iii) foreign materials may be needed at the interface to enable fusion bonding. Based on heat generation mechanisms, fusion bonding is further separated into four types: i) bulk heating, ii) frictional heating, iii) electromagnetic heating, and iv) two-stage techniques [32]. Among all these fusion bonding techniques, resistance welding and induction welding, belonging to electromagnetic welding, as well as ultrasonic welding, a member of friction welding, are the topics of much interest in recent years [31,33–68].

Since joints are typically the weakest points in assembled composite structures, during use, they will fail first. Therefore, it is essential to develop non-destructive testing (NDT) and structural health monitoring (SHM) techniques, which can not only provide a warning at the initial stage of damage, but also, effective and reliable information regarding joint condition throughout service life to initiate repair or replacement when necessary. Failure modes in mechanically fastened composite joints include a combination of matrix cracking, delamination, fiber breakage, bearing, net-tension, shear-out, and tear-out failure. In adhesively bonded composite joints, failure can be divided into two categories: i) adherend failure, including interlaminar delamination, matrix cracking, fiber breakage, and adherend fracture and ii) adhesive failure, such as cohesive failure and adhesive/adherend interfacial failure [69]. Major failure modes within welded composite joints typically include interfacial failure, cohesive failure, and intralaminar failure (e.g., fiber–matrix debonding, fiber breakage, or tearing of the laminates). In addition to failure modes, bond line defects resulting from the manufacturing process should be considered, for example, unbonded areas, weak "kissing" bonds, and loose fasteners. Given the wide range of failure modes and defects for each joint type, developing SHM techniques capable of identifying them individually is challenging.

When performing damage detection, damage monitoring methods for composite joints should consider three aspects: i) type of damage, ii) location of damage (e.g., within the joint or in the adherends), and iii) severity of damage (e.g., crack length, unbonded area). Over the last years, several SHM methods have been used for composite joints, which can be divided into two general categories, as detailed in Table 1: i) intrinsic sensing (directly embedded at the joint interface) and ii) extrinsic sensing (monitoring device placed outside the interface). Embedded methods include, among others, fiber optic sensors (FOSs), piezoelectric sensors, and nanocomposite-based monitoring. The latter typically involves a polymer adhesive or film, modified with electrically conductive nanoparticles, placed at the bond line. It is one of the most diverse approaches in terms of materials in recent literature. External NDT techniques for monitoring composite joints include acoustic emission (AE), guided waves, structural vibrations and acoustics, laser shock adhesion test, ultrasonic scanning, thermography, dielectric sensing, and piezoelectric sensors. Table 1 lists some of the main features, advantages, and disadvantages for each method, as applied to composite joints, including frequency range (if relevant) and inspection area. Local and global inspection techniques are classified with respect to the overall joined structure's dimensions. Local techniques can monitor a specific area along the joint and detect small defects like cracks or disbonds, while global methods cover a larger joint area, but may have lower resolution.

A study of the existing work on damage monitoring of fiber-reinforced polymer joints shows that there is still a lack of comprehensive and state-of-the-art literature review in this critical area. Towards this end, in this paper, advances in intrinsic and extrinsic monitoring methods for adhesively bonded, mechanically fastened, and welded composite joints, including repair patches, were scrutinized. We define a composite joint as having at least one adherend made from fiber-reinforced polymer. Main types of embedded sensors at the joint interface were reviewed, focusing first on nanocomposite-based sensing approaches (Section 2), as they incorporate a wide range of material types. They are followed by Section 3, which covers other intrinsic methods, such as fiber optic and piezoelectric sensors. Then, valuable research on extrinsic techniques for SHM of composite joints are summarized in Section 4. At the beginning of each sub-section, a summary of the main applications (joint types) for the corresponding SHM technique is included. Finally, through an analysis of gaps and limitations, future work needed to explore and improve real-time damage monitoring methods for composite joints is identified.

2. Nanocomposite-based monitoring

2.1. Theory and background

Incorporation of electrically conductive nanoparticles, like carbon nanotubes (CNTs), into non-conductive polymer matrices can create electrical networks, which will be disrupted under mechanical strain. For instance, upon tensile loading, the distance between CNTs embedded in the polymer matrix increases, leading to a rise of electrical resistance in the nanocomposite. The relationship between the change of electrical resistance ($\Delta R/R_0$) and applied strain (ε) is known as the gauge factor (G_F), the piezoresistive sensitivity of materials, and is written as follows [177]:

$$G_F = \frac{\Delta R/R_0}{\varepsilon} \tag{1}$$

Where R_0 is the baseline resistance at time t_0 and ΔR is the resistance difference between time t and t_0. As a consequence, it has led to an increased interest in damage detection in composite laminates with nanocomposite matrices or interleaved films, with potential for in-situ self-sensing of composite joints without using additional, external sensors. In this respect, the electrical resistance measurement method is a promising alternative to NDT techniques due to its simplicity and integration at the bond line through nanocomposite adhesives or films. Several related comprehensive literature reviews have been reported in the past five years, focusing on damage monitoring of composite laminates. For example, Park et al. [79] presented a detailed review on electrical resistance measurements for damage self-sensing and interfacial evaluation of CNT- or carbon fiber (CF)-reinforced composites subjected to mechanical loading. It covered studies based on experimental research. Studies on CNT-based damage monitoring using electrical resistance measurements for CNT-dispersed single fiber composites and laminated composites via physical or chemical dispersion methods under different loading conditions were summarized in [85]. It indicated that CNT concentration and dispersion level played a crucial role in damage sensing for composites. Zhang et al. also presented a summary of other damage detection sensing techniques using surface-mounted or embedded sensors. In addition, they provided a systematic review on damage detection under standardized tests, contributing to a good understanding and providing confidence for industrial applications.

The next sub-sections summarize most recent advancements in nanocomposite-based damage monitoring for various joint types: adhesive, bolted, and welded joints. Table 2 lists main materials (for nanocomposite and adherend), joints parameters (bond line thickness and configuration), characterization tests, and lap shear strength (LSS). It highlights that most studies have been conducted on adhesively bonded joints for thermoset composites, while research on mechanically fastened and welded joints is minimal.

Table 1
Summary of sensing technologies for damage monitoring in composite joints.

Technology	Main features and advantages	Main disadvantages	Ref.
Intrinsic methods (embedded sensing)			
Nanocomposite-based sensing Inspection area: local / global	• Minimally invasive with polymer matrix similar to adherends • Possibility of in-situ, real-time damage monitoring • Can provide more sensitivity than conventional SHM techniques	• May affect mechanical performance at high nanofiller content • Effectiveness depends on filler content and dispersion • Limitations regarding detection of damage location and type	[5,11,12,15,16,19,22,70–86]
Fiber optic sensor (FOS) Inspection area: local / global	• Accurately measures strain and temperature • Can be locally embedded at interface and spatially distributed • Potential for detection of damage type, size, and location • Possibility of in-situ, real-time damage monitoring • Suitable for large structures (km)	• May affect mechanical performance • Relatively expensive • Potentially complex systems and data analysis	[1,2,6,13,23–26,87–107]
Electromechanical impedance (EMI)) (e.g., piezoelectric sensor) Inspection area: local / global	• Potential to detect “kissing” bonds in adhesive joints • Can identify damage initiation based on location • Possibility of in-situ, real-time damage monitoring	• Multiple sensors required to monitor large structures • May affect mechanical performance	[14,108,109]
Other methods: Z-pins, Eddy current (EC) sensing films Inspection area: local	• Z-pins act as crack-arresting mechanism • Potential for crack growth monitoring (EC films) • Possibility of in-situ, real-time damage monitoring	• Time-consuming installation (Z-pins and EC films) • Complex real-time data acquisition and implementation • Limited penetration depth (EC films)	[110–112]
Extrinsic methods (external non-destructive testing)			
Technology	**Main features and advantages**	**Main disadvantages**	**References**
Acoustic emission (AE) Frequency range (Hz): 10^4-10^6 Inspection area: local / global	• High sensitivity • Potential for detection of damage type and location • Can be integrated into existing structures for real-time • Fully passive method	• Complex data analysis for damage classification • No indication of damage severity (e.g., disbond length, etc.) • May be sensitive to external noise	[74,113–128]
Acousto-ultrasonic wave (e.g., guided waves) Frequency range (Hz): 10^4-10^6 Inspection area: local / global	• High sensitivity • Can be implemented into existing structures for real-time monitoring • Sensitive to geometric changes at bond line	• Complex implementation and data analysis for damage localization, type, and severity • Difficult to analyze complex structures as sensor configuration affects response	[7,48,96,129–147]
Structural vibrations and acoustics Frequency range (Hz): 1–10^4 Inspection area: local / global	• Low level of measurement noise • Can detect defect location and size • Possibility of real-time damage monitoring	• Limited sensitivity compared to higher-frequency methods • Defect position and structure design may affect effectiveness	[148–153]
Laser shock adhesion test Inspection area: local	• Non-contact • Can detect weak bonds	• Can damage specimens • Limited to adhesive joints	[154–159]
Electromechanical Impedance (EMI) (e.g., piezoelectric sensor) Frequency range (Hz): 10^3-10^5 Inspection area: local / global	• Possibility of in-situ, real-time damage monitoring • Can quickly inspect long range defects	• Response can be affected by joint boundaries • Multiple sensors required to monitor large structures • Difficult to analyze complex structures as sensor configuration affects response	[160–162]
Ultrasonic scanning and phased array Frequency range (Hz): 10^5-10^7 Inspection area: local / global	• Can be used on large structures • Direct visualization of bond line quality/defects	• Generally cannot detect kissing bonds • Limited damage type detection • Challenging application for real-time, online monitoring • Physical access to joint area required	[25,163–168]
Thermography Inspection area: local / global	• Non-contact • Capable of inspecting large areas	• Generally cannot detect kissing bonds • Challenging application for real-time monitoring of existing structures • Physical access to joint area required	[74,169–172]
Digital image correlation (DIC) Inspection area: local / global	• Non-contact • Capable of inspecting large areas • Potential to detect kissing bonds	• Extensive sample preparation • Physical access to joint area required • Limited damage type detection	[173]
Others (dielectric-based, heterodyning) Inspection area: local / global	• Relatively low voltage excitation signal (heterodyning) • Straightforward selection of excitation frequencies (heterodyning) • Can monitor water uptake in composites and joints (dielectric-based)	• Generally cannot detect kissing bonds or damage severity • Adherends must be electrically conductive (dielectric)	[174–176]

Table 2
Summary of materials and process parameters for nanocomposite-based joints monitoring methods. NC: nanocomposite, t: bond line thickness, LSS: lap shear strength.

Joint type	NC matrix	NC filler (wt%)	Adherends and joint geometry	t (mm)	Characterization tests	LSS (MPa)	Ref.
Adhesive	FM 300 K	NC7000 MWCNTs (0.1 wt%)	Carbon fiber reinforced polymer (CFRP) Standard Mode-II coupon Skin-stringer element	N/A	• Bending tests • Electrical resistance measurements • Scanning electron microscopy (SEM)	N/A	[80]
Adhesive	FM 300 K	NC7000 MWCNTs (0.1 wt%)	CFRP Standard Mode-I coupon Skin-stringer element	N/A	• Peeling tests • Electrical resistance measurements • SEM	N/A	[22]
Adhesive	FM 300 K	NC7000 MWCNTs (0.1 wt%)	CFRP Single lap	N/A	• Fatigue tests • Voltage measurements • Optical microscope • SEM	N/A	[5]
Adhesive	Epoxy adhesive (Araldite LY 5052/Aradur 5052)	MWCNTs (0.5 wt%)	CFRP prepreg Single lap	0.76	• Impedance spectroscopy measurements • Lap shear tests • Transient infrared thermography • SEM	8.86 (no sensor) 8.19 (with sensor)	[12]
Adhesive	Hysol ® EA 9396	CVD-grown MWCNTs (1.0 wt %)	Vinyl ester/glass composite-stainless steel Single lap	0.762	• Monotonic and incremental cyclic tensile tests • Electrical resistance measurements • Acoustic emission	N/A	[78]
Adhesive	Hysol 9309.3NA, nonwoven aramid fabric 20601	CNTs	Carbon fiber (CF)/epoxy resin-steel Single lap	2	• Monotonic and incremental cyclic tensile tests • Electrical resistance measurements	14.4 (control specimens) 9.7 (adhesive insulated specimens) 14 (fabric insulated specimens)	[15]
Adhesive	Epoxy adhesive (KSR 177) & hardener (G 640)	CM 95 CNTs (2 wt%)	Carbon/epoxy-Al Single lap	2	• Tensile tests • SEM • Fatigue tests • Equivalent resistance and capacitance measurements	N/A	[16]
Adhesive	Epoxy resin (Araldite LY 556) & hardener (XB 3473)	NC7000 MWCNTs (0.1 wt%)	CFRP-Ti6Al4V Single lap	N/A	• Tensile tests • Double cantilever beam tests • Electrical resistance measurements	Slightly decreased compared to neat adhesive Increased fracture toughness	[71]
Adhesive	Cytec FM 300 epoxy film adhesive	Highly aligned CNT-single layer web (CNT-SLW)	Glass fiber (GF)/epoxy Single lap	0.26	• Quasi-static cyclic tensile tests • Electrical resistance measurements • FESEM	Slightly increased compared to neat adhesive	[19]
Adhesive	Epoxy adhesive Bisphenol epoxy resin (HZ1-A) & hardener (HZ1-B)	MWCNT & carbon black (CB) (2 wt%)	CFRP laminate-high-strength steel Single lap	2	• SEM • Two-electrode method • Electrical resistance measurements • Tensile tests	Increased by 3.12 % in CB, 37.5 % in CNT:CB = 1:3, and 62.5 % in CNTs	[84]
Adhesive	Bisphenol-A	MWCNTs & graphene (GNs)	GF/epoxy prepreg Single lap	0.105	• Quasi-static and cyclic shear tests • Electrical resistance measurements • FESEM	0, 5, and 10-GC/epoxy changed by + 42 %, +10 %, and −3.5 % compared to neat adhesive	[83]
Adhesive	Epoxy resin (EPON LVEL 828)	Tuball SWCNTs (0.5 wt%)	CFRP prepreg Scarfed joints	N/A	• Cyclic fatigue tests • Electrical resistance measurements • DIC measurements • SEM	N/A	[11]
Adhesive	Epoxy resin (EPON resin 828)	Tuball SWCNTs (0.5 wt%)	Glass fiber reinforced polymer (GFRP) Biaxial plates	N/A	• Electrical resistance measurements • Drop weight impact tests • Ultrasonic measurements • Pulse-echo method • Optical microscope	N/A	[70]
Adhesive	Epocast 52 A/B	MWCNTs (0.5 wt%)	CFRP prepreg Four-layer patch	N/A	• Fatigue mechanical tests • Electrical potential change monitoring • Acoustic emission	N/A	[74]

(*continued on next page*)

Table 2 (*continued*)

Joint type	NC matrix	NC filler (wt%)	Adherends and joint geometry	t (mm)	Characterization tests	LSS (MPa)	Ref.
Adhesive	Bisphenol A '105' & harder '206'	Vapour-grown carbon nanofibers (CNFs) (0.7 wt%)	CF/epoxy prepreg Double-cantilever beam	2	• Lock-in thermography • Fatigue tests • Four probe resistance measurements	N/A	[75]
Adhesive	Hexcel M26T epoxy	Nickel-coated carbon veil	GFRP Single lap	0.11	• Electrical resistance measurements • Thermography • Short beam interlaminar shear tests • Quasi-static tensile tests • DIC measurements	No significant difference with and without sensor adhesive	[86]
Bolted	Bisphenol-fepichlorohydrin epoxy (EPON 862)	MWCNTs (0.5 wt%)	Glass/epoxy-CNT/GF Single lap Double lap	N/A	• Quasi-static monotonic and increasing cyclic tensile tests • Electrical resistance measurements	N/A	[81]
Bolted	Bisphenol-f epoxy monomer (EPON 862)	CNTs (0.75 wt%)	CNT/E-glass/vinyl eater-fiberglass composite Double lap	N/A	• Quasi-static monotonic and cyclic tensile tests • Electrical resistance measurements	N/A	[73]
Bolted	Woven GF cloth (WGF)	MWCNTs	WGF/epoxy T-joint		• Tensile tests • SEM • Electrical resistance measurements	Increased compared to neat composite	[82]
Welded	PP	MWCNTs (15 and 20 wt%)	GF/PP Single lap	0.5	• Tensile tests • Bending tests • Electrical resistance measurements	Slightly decreased compared to neat PP films	[72]
Welded	PP	MWCNTs (15, 20, and 25 wt%)	GF/PP Single lap	0.5	• Tensile tests • Electrical resistance measurements • SEM	Slightly decreased compared to neat PP films	[76]

2.2. Application to adhesive joints

2.2.1. CNT/adhesive-based damage monitoring

Introducing CNTs into epoxy adhesive can significantly improve the electrical conductivity of the latter. This feature is used to evaluate the ability of CNT networks to detect and monitor, in-situ, the onset and propagation of damage in adhesively bonded joints through various testing techniques. Some efforts have been made in composite/metal hybrid joints, which have employed CNT/adhesives for damage sensing [16,71,78,84]. However, it is worth noting that the majority of previous research directly introduced CNTs into the adhesive, which usually resulted in an increase in viscosity, affecting dispersion, and leading to a decrease in mechanical properties (such as strength of single lap joints). To overcome these issues, Doshi et al. [15] proposed a novel method by applying a CNT-based sensing layer in adhesively bonded CF composite/steel joints for damage detection. A well-mixed CNT sizing (sizing:ultra-pure water = 1:2) was deposited onto a nonwoven aramid fabric for 20 min and then dried in an oven for 30 min at 150 ℃. Two approaches to insulate the sensing layer from the steel adherend were investigated, as shown in Fig. 1: i) a cured adhesive layer and ii) a non-conductive fabric. Fabric insulation showed no significant effect on lap shear strength (LSS) subjected to monotonic tension loading. Additionally, there was no damage at the sensing layer for samples insulated by non-conductive fabric, which also presented a more linear resistance response than adhesive insulation under gradually increasing cyclic loading. This demonstrated that CNT-based sensing layers might have the ability to identify failure modes within the bond line.

With the increase of industrial demand for lightweight and high-strength components, adhesively bonded fiber-reinforced composite-to-composite joints are the subject of high interest nowadays. In this regard, SHM techniques for composite/composite joints, especially CNT-based monitoring methods, have gained momentum in the past five years [5,11,12,19,22,70,74,80,178]. For example, Sánchez-Romate et al. [178] developed a CNT doped adhesive film by dispersing CNTs in water with 0.1 wt% sodium dodecyl sulfate (SDS) surfactant under sonication and applied it to join CFRP adherends. They found that 20 min sonication produced good CNT dispersion, and SDS helped disaggregate CNTs, while CFRP joints with 0.25 wt% SDS showed the highest LSS and electrical conductivity among 0, 0.1, 0.25, and 1 wt% SDS. Following adhesive film development, fracture growth monitoring for single lap CFRP joints with CNT doped adhesive films via electrical resistance change under fatigue loading was discussed by this research group [5]. However, achieving an excellent dispersion of randomly oriented CNTs in solvent remains a challenge because of their aggregation and increased adhesive viscosity. Toward this end, a method positioning highly aligned CNT single layer web (CNT-SLW) over adhesive film sandwiched between two glass fiber (GF) laminate adherends was proposed to detect damage initiation and progression in single lap joints subjected to quasi-static and cyclic loading in [19]. The authors placed horizontally drawn CNT-SLW on adhesive film in a direction parallel or perpendicular to tensile loading. Under quasi-static loading, joints bonded with CNT-SLW perpendicular to loading displayed a very small change in resistance compared to the parallel direction, which showed a high sensitivity of $\Delta R/R_0$ (%) at damage initiation, damage accumulation, and final failure jumping to 1631 %. These two CNT-SLW sensing mechanisms are clearly depicted in Fig. 2. Moreover, an example of sensor response for displacement-controlled experiments with a maximum displacement of 1.5 mm (Fig. 3a) was also presented. In cycles 1 ~ 10, the maximum resistance increased linearly with a large slope, indicating that numerous CNTs were disconnected, while minimum resistance was almost constant, suggesting CNTs reconnected during unloading due to their high alignment. Detailed damage information is observed from the magnified image in Fig. 3b. On the contrary, CNT-SLW perpendicular to loading showed poor sensitivity under both quasi-static loading and cyclic loading. Highly aligned CNT-SLWs are promising for SHM due to their higher

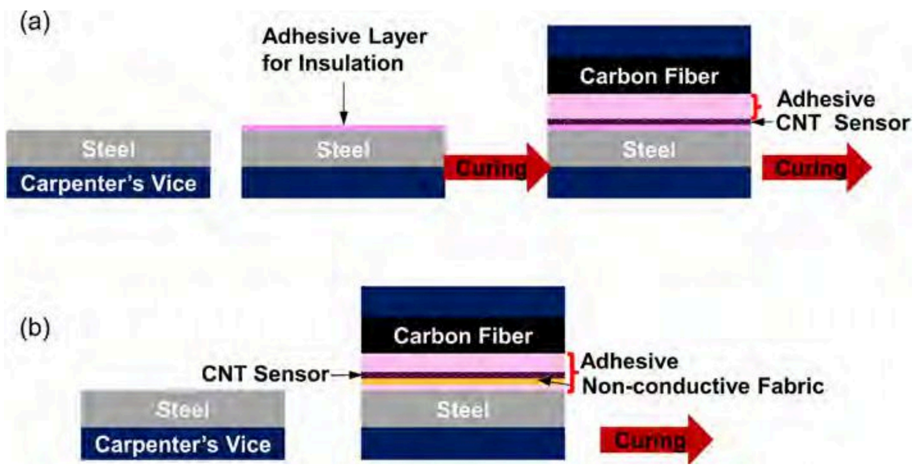

Fig. 1. A schematic diagram showing two approaches to insulate CNT sensor layer from the steel adherend: (a) adhesive-insulated adherend with two-step curing and (b) fabric-insulated adherend with one-step curing [15].

cyclic stability and sensing sensitivity compared to conventional CNT dispersion mentioned above.

Additionally, several research groups have shown interest in damage monitoring of complex structural composite joints, such as scarfed joints and skin-stringer assemblies. Augustin et al. [11] manufactured a 0.5 wt % single wall carbon nanotube (SWCNT) modified epoxy adhesive film using a three-roll mill and applied it to scarfed CFRP joints with a scarf angle of 2.86°, where inkjet-printed conductive paths were placed on opposite sides of the film. By this means, crack initiation and growth subjected to cyclic loading were detected via electrical resistance measurements and translated into heat maps. An example of electrical resistance change using damage mapping is shown in Fig. 4. They pointed out that crack initiation could be detected by a sudden increase in electrical resistance, while a continuous increase in resistance over lifetime represented crack growth. Furthermore, interpreting the difference in resistance between different conductive paths could be used as a basis for determining the crack location. Augustin et al. [70] relied on this SWCNT-modified adhesive film to investigate the damage detection and localization for GFRP plates under impacts via inkjet-printed conductive paths. After that, CNTs doped adhesive films proposed in [178] were used for monitoring damage propagation of co-bonding and secondary bonding of skin-stringer elements with two different artificial defects, namely liquid release agent and Teflon insert, through electrical resistance measurements subjected to peeling tests. For the electromechanical curves of the two bonding methods, three regions were established, corresponding to different defect mechanisms. No matter which bonding technology the skin-stringer elements was bonded with or defect types attached, a sudden decrease in mechanical loading was always accompanied by a sharp jump in resistance [22]. Sánchez-Romate et al. [80] also investigated the detection capability of

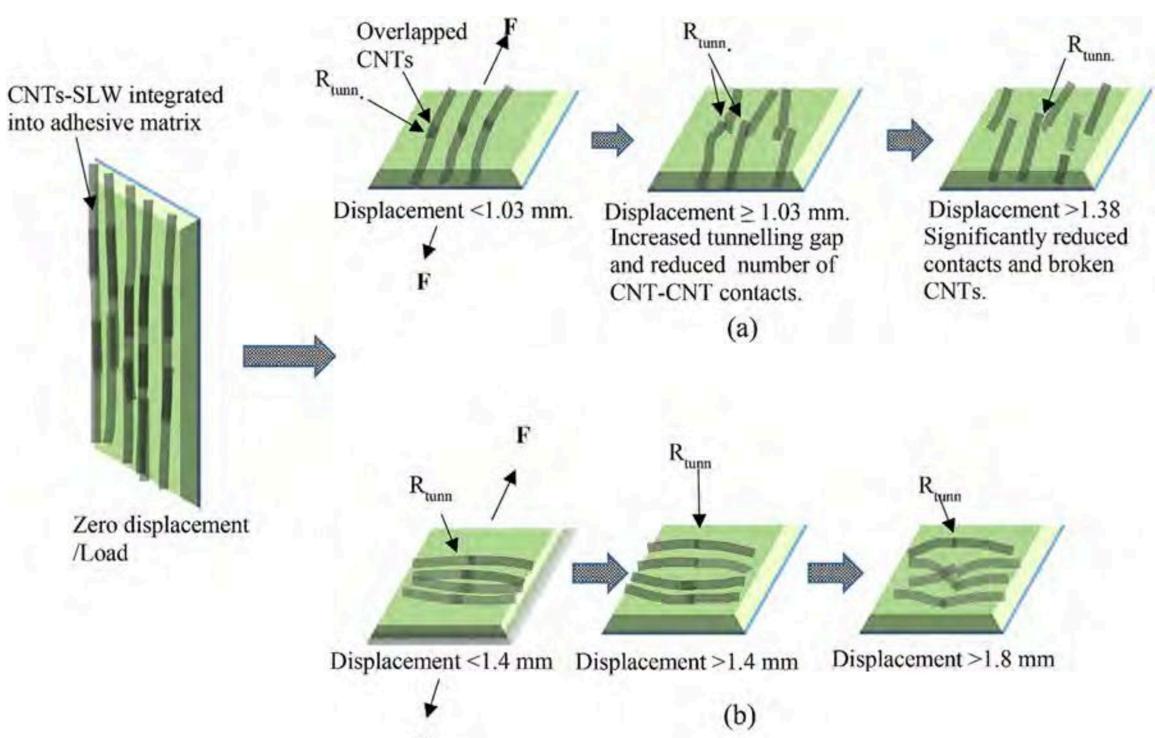

Fig. 2. Representation of the damage sensing mechanism for CNT-SLW (a) parallel and (b) perpendicular to load direction with increasing end-displacement (deformation) (Reproduced with permission from [19]).

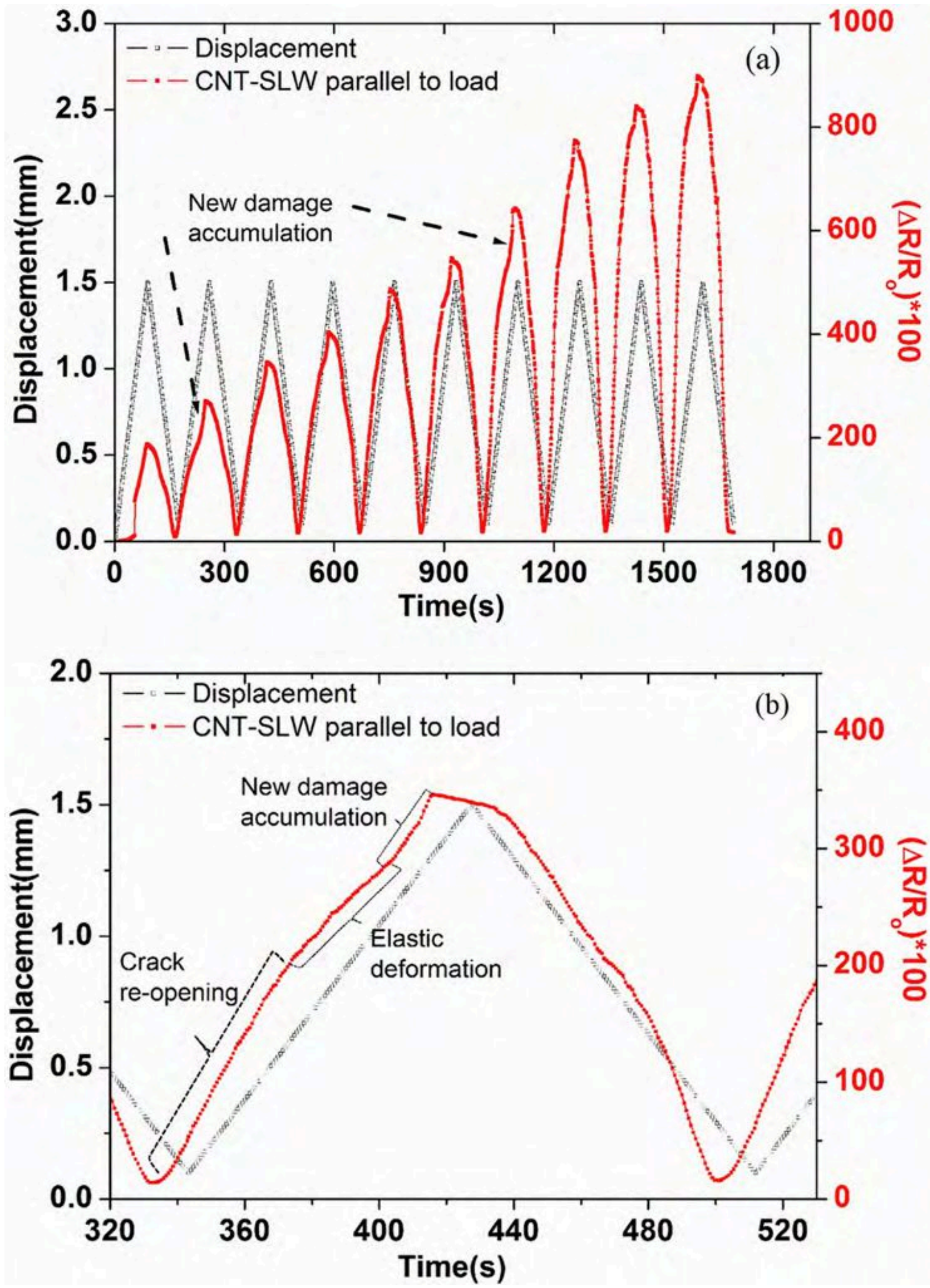

Fig. 3. (a) Sensor response at a maximum end-displacement well above the damage initiation threshold and (b) expanded view of subsequent cycle highlighting the re-opening of a crack and formation of new damage (Reproduced with permission from [19]).

the same CNTs doped adhesive film for crack growth in Mode-II coupons and skin-stringer sub-elements under static bending loading until failure. They found that incorporating CNTs increased Mode-II energy fracture, resulting in a slower crack propagation compared to the neat adhesive. Furthermore, electrical resistance increased with crack opening in both CFRP structures due to the breakage of conductive pathways, showing a potential for SHM applications.

2.2.2. Hybrid nanoparticle-based damage monitoring

As aforementioned, CNTs show potential for SHM of adhesive joints due to their excellent electrical properties with a low percolation threshold, but cost and tendency to create large agglomerates due to their high aspect ratio are notable issues [179], as well as relatively poor sensitivity [180]. Several researchers have proved that incorporating hybrid conductive fillers into adhesives can effectively compensate for the limitations of CNTs. For instance, Ke et al. [181] combined CNTs and carbon black (CB) due to the latter's low cost and high sensitivity to tune the electrical conductivity and piezoresistive sensitivity of poly (vinylidene fluoride) (PVDF) and found that a high CNT/CB ratio provided a high electrical conductivity, while a low CNT/CB ratio led to a high piezoresistive sensitivity. Studies on mechanical properties [21,84,179], rheological properties[182], and strain sensing behaviors [180] of CNT/CB-based adhesive were also reported. Recently, Yang et al. [83] employed a filtration method to develop CNT/epoxy adhesives with 0, 5, and 10 wt% of layered graphene nanoplates (GNs), namely 0-GC/epoxy, 5-GC/epoxy, and 10-GC/epoxy. This approach introduced not only line-to-surface contacts between CNTs and GNs, but also surface-to-surface contacts between GNs, except for the original point-to-point contacts between CNTs, allowing to improve the monitoring sensitivity for adhesively bonded GF/epoxy joints. Under quasi-static shear loading,

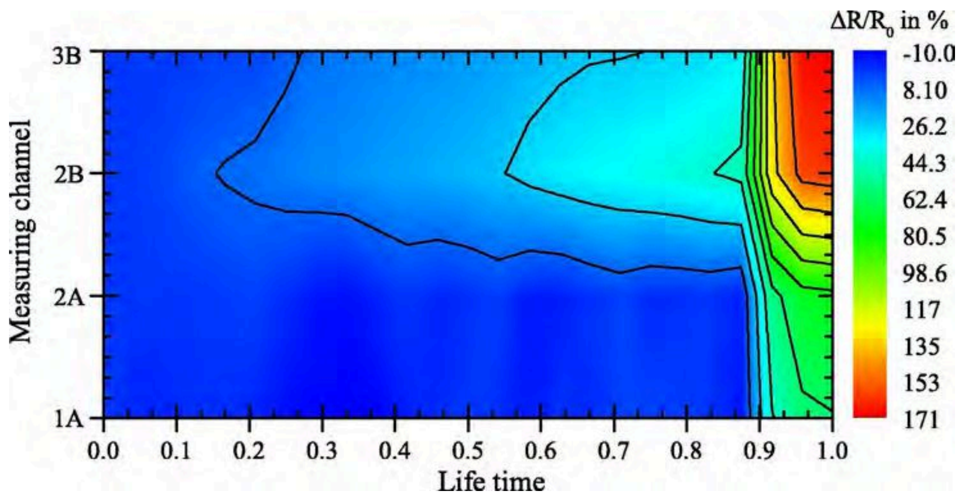

Fig. 4. Heat map showing electrical resistance changes of the four measured channels over the life time for a specimen with crack initiation and final failure at same location (Reproduced with permission from [11]).

electrical resistance change exhibited a slow linear increase with shear strain, about 1.0–4.0 % for three types of GC/epoxy at undamaged stage. When shear strain reached a certain value, resistance changes increased suddenly, indicating damage initiation and conductive networks crack, as shown in Fig. 5. In Fig. 5e, 5-GC/epoxy and 10-GC/epoxy had a reduced shear strain γ compared to 0-GC/epoxy, while their $\Delta R/R_0$ (%) were as high as 191 % and 140 %, respectively. From this perspective, 5-GC/epoxy film was more sensitive than the other two, validated by acoustic emission energy. Moreover, 5-GC/epoxy films provided a higher stable sensitivity of 160 % $\Delta R/R_0$ (%) than 0-GC/epoxy films [32 % $\Delta R/R_0$ (%)] under cyclic shear loading when shear damage began. These proposed hybrid nanocomposites showed a new perspective and applicability for damage monitoring of adhesively bonded composite joints.

2.3. Application to mechanically fastened and welded joints

2.3.1. Damage monitoring for mechanically fastened composite joints

Since mechanically fastened composite joints have high stress concentration, they are susceptible to damage around fasteners. Therefore, it is critical to evaluate their failure behavior. However, external NDT techniques usually require disassembly of mechanically fastened joints, resulting in a long downtime. To this end, CNTs were gradually introduced into composites for sensing. For example, Thostenson and Chou [81] detected local damage of composites and bolt loosening subjected to quasi-static monotonic tensile loading and increasing cyclic loading with mixed CNT/epoxy resin infused through the glass fibers. Fig. 6a illustrates unidirectional GF/epoxy composite specimens with single-lap and double-lap joints fastened by fully threaded steel bolts and flange hex nuts. In that work, a stick/slip fracture appeared in these two types of lap joints under loading (Fig. 6b), which was different from the load curves of adhesively bonded joints after the initial damage, as discussed in Fig. 5. Furthermore, every drop in load was accompanied by a jump in electrical resistance. It was worth noting that the whole resistance change of the single-lap joints was very small, less than 3 %. On one hand, it might be caused by the direct contact between bolt and composite laminate, leading to new conductive paths. On the other hand, thin composite bending reduced the electrical resistance. However, double-lap joints addressed each of these shortcomings. In this respect, the same research group continued their study on CNT/resin-based bolted cross-ply double-lap shear E-glass composite joints under monotonic and cyclic tensile loading using electrical resistance measurements [73]. Different from unidirectional joints with a shear-out failure mode due to low shear strength along the fiber direction, cross-ply composite joints exhibited complex damage modes, such as net-tension, bearing, shear-out, and tear-out, which might be associated with interlaced fiber direction and complex internal networks. In [73], Friedrich et al. investigated the correlation between electrical resistance response and damage of joints through ultrasonic C-scan and optical microscopy. Electrical resistance measurements were more sensitive to matrix cracks and delamination between 0° and 90° layers due to their disturbance on CNT conductive networks compared to bearing, shear-out, as well as tear-out failures, which did not severely disturb the conductive networks, giving rise to weaker sensitivity to resistance data. Therefore, CNT networks can be excellent candidates for SHM of mechanically fastened joints.

More recently, Wan et al. [82] embedded a nanocomposite-based sensor, MWCNT-coated woven GF cloth (MWCNT@WGF), into the bottom and the web of bolt-fastened WGF/epoxy T-joints for damage monitoring under tensile loading. As depicted in Fig. 7, resistance Tunnel-2, along the bottom of the T-joint, showed a first sharp growth due to the onset of delamination, leading to the MWCNT@WGF sensor cracks. Under continuous loading, this propagation would decrease when the delamination encounters bolts, consequently, followed by a slight change in the resistance curves. However, since there was delamination along the web direction, corresponding to resistance Tunnel-1, the latter kept increasing until final failure. In addition, their method also demonstrated the ability to significantly enhance the strength of T-joints.

2.3.2. Damage monitoring for welded composite joints

Unlike adhesively bonded joints, there is very limited published research related to nanocomposite-modified welded composite joints, especially for both induction and resistance welding. Farahani and Dube [42] developed heating elements (HEs) using Ag-coated carbon nanofibers (CNFs), Ni-coated CNFs, and Ag-coated CNFs with magnetic Fe_3O_4 nanoparticles casted on a pure polyphenylene sulfide (PPS) film used for induction welding. In that work, the mechanical performance and welding quality of unidirectional and cross-ply CF/PPS joints, as well as heating behavior of different HEs, were investigated and discussed. The following year, Farahani et al. [43] continued their research on PPS films casted by nAg as a HE. Apart from this application, nanocomposites were incorporated into resistance welding as well. Brassard et al. [33] examined the mechanical properties and welded surface of resistance welded single lap shear CF/poly (ether ether ketone) (PEEK) joints with MWCNT-based polyetherimide (PEI), as a new HE. Numerical research regarding enhancing mechanical performance through study of welding parameters and temperature distribution during

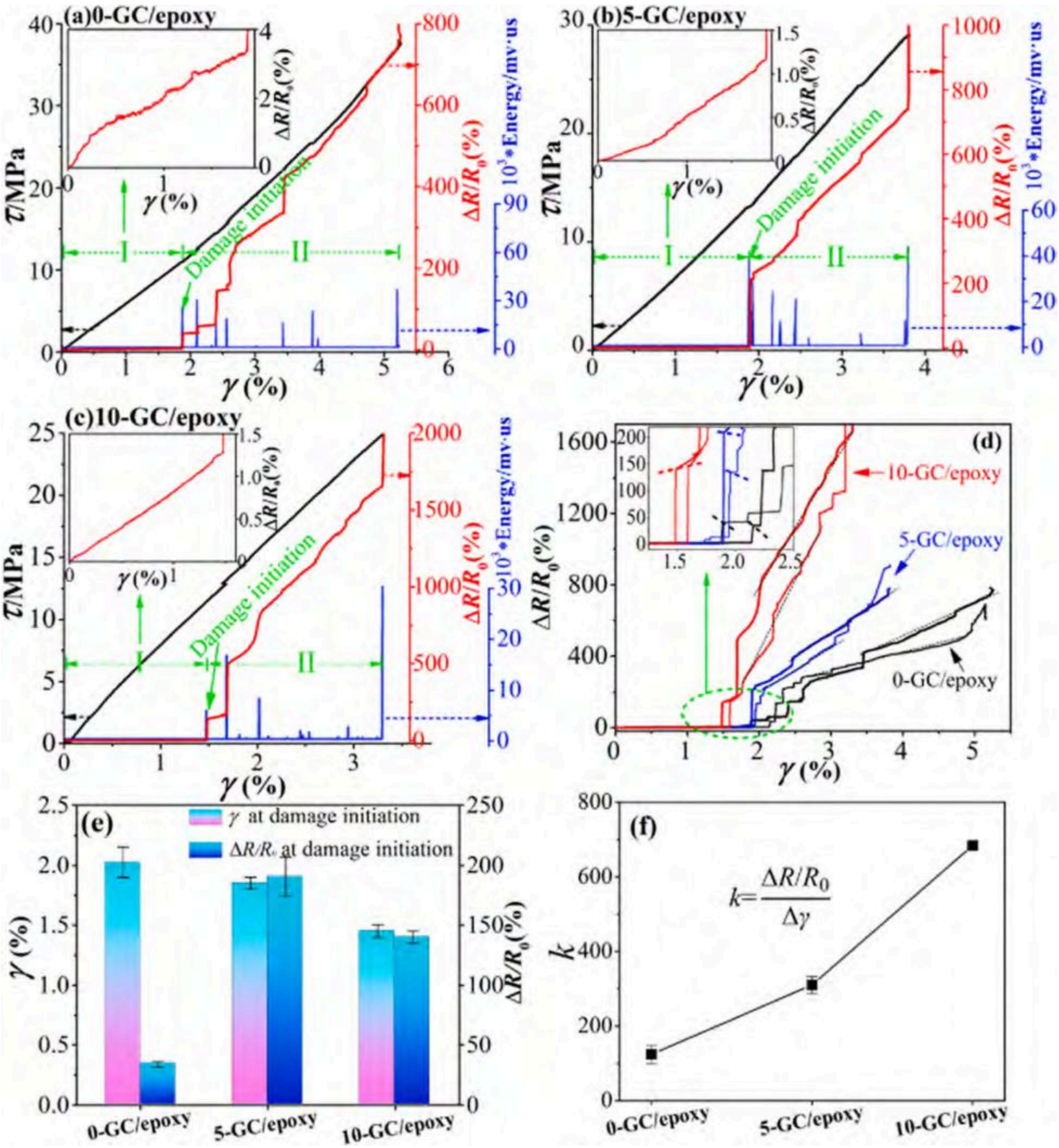

Fig. 5. τ, $\Delta R/R_0$ (%), and AE energy versus γ (%) for (a) 0-GC/epoxy, (b) 5-GC/epoxy, and (c) 10-GC/epoxy obtained from the quasi-static loading tests; (d) comparisons of the $\Delta R/R_0$ (%)-γ (%) curves; (e) comparisons of the average γ and $\Delta R/R_0$ (%) obtained at the damage initiation; and (f) the average sensitivity coefficient of the GC sensors (Reproduced with permission from [83]).

welding with a finite element model was also conducted by the same group [34]. However, the presented work all focused on studying welding parameters and mechanical properties of welded joints. To the authors' knowledge, nanocomposite-based damage monitoring in welded composite joints has never been done in induction welding and resistance welding.

Similarly, although a large amount of research has been conducted in ultrasonically welded composite joints in recent years, most work focuses on the welding process, welding quality, and mechanical behavior of the joints [3,4,27,28,46,47,49,55,61,62,65,67,68,183–187]. Therefore, a comprehensive understanding of the application of nanocomposites for damage sensing of ultrasonically welded joints has not been reported. Recently, multifunctional films containing MWCNTs dispersed into a thermoplastic matrix were proposed to enable ultrasonic welding, SHM, and resistive heating for disassembly of welded thermoplastic composite joints [72,76,77,188,189]. For instance, Frederick et al. [72] manufactured 0.06, 0.25, and 0.50 mm-thick 15 and 20 wt% MWCNT/polypropylene (PP) films via compression molding. The authors confirmed that electrical resistance changes were linked to applied strain to the films through DMA tests under tension. Films with a thickness of 0.50 mm were selected to successfully weld GF/PP adherends in a single lap configuration. In this respect, electrical resistance was measured when welded joints were subjected to cyclic bending loading, showing a clear correlation with bending duration.

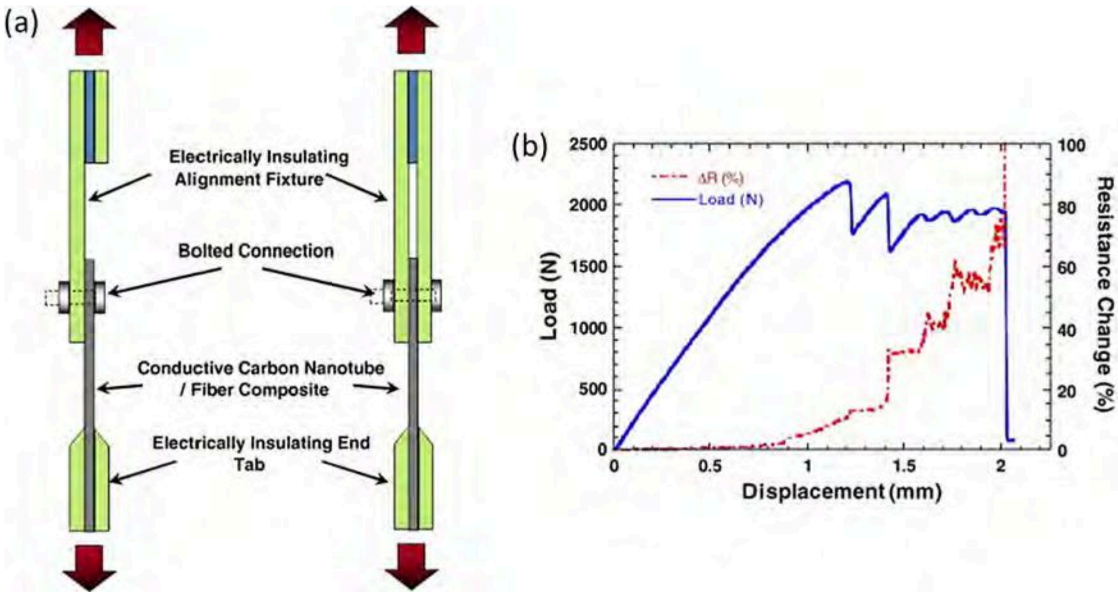

Fig. 6. (a) Diagram showing the configuration and test setup of specimens in single (left) and double (right) lap geometries and (b) load–displacement and resistance curves for a double-lap joint configuration, showing the complete resistance response after initial failure to ultimate fracture (Reproduced with permission from [81]).

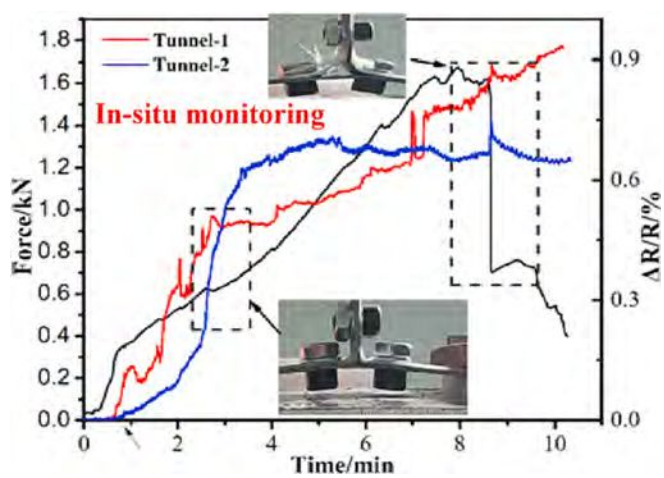

Fig. 7. In-situ monitoring of bolt-fastened WGF/epoxy T-joint (Reproduced with permission from [82]).

Based on these results, Li et al. [76] investigated the damage sensing capabilities of 0.50 mm-thick 15, 20, and 25 wt% MWCNT/PP films in ultrasonically welded GF/PP joints, subjected to tension loading until failure. During this process, the electrical resistance at the welded interface was measured. They reported that every sudden drop in stress inevitably led to a significant jump in resistance for all joints welded with 15 and 20 wt% MWCNT/PP films, while 25 wt% MWCNT/PP film-welded joints failed immediately when stress reached its maximum, leading to a sharp resistance increase, attributed to a brittle interface. Overall, 15 and 20 wt% MWCNT/PP multifunctional films developed in that work presented a novel method for damage monitoring of thermoplastic composite joints. However, for those particular materials, the nanocomposite films led to a decrease in lap shear strength (less than 20 %), which needs to be addressed in future work. The potential for in-situ strain and damage monitoring of nanocomposite films (based on 5, 10, 15, and 20 wt% MWCNTs) under static and cyclic flexural loads was also studied for welded GF/PP single lap joints (SLJs) and 3-point bending joints (3PBJs) [189]. The crack initiation and propagation at the welded interface can lead to resistance changes and double-film 3PBJs showed a high sensitivity with $\Delta R/R_0$ (%) up to 300 % subjected to monotonic 3PB loads. Furthermore, 15 wt% MWCNT/PP films embedded away from the neutral axis also presented sensing capability under cyclic flexural loading. It is worth noting that nanocomposite films increased the flexural strength by an average of 20.6 %.

3. Embedded sensors for damage monitoring

3.1. Fiber optic sensors (FOSs)

Fiber optic sensors (FOSs), including distributed FOS (DFOS) and fiber Bragg grating (FBG) sensors, have been used for SHM of various types of composite joints: i) adhesively bonded GFRP and CFRP joints, including single, double, and step lap joints [1,2,6,13,23,87,88,90,97,99–101] under static and cyclic loading [24,25,96,98,106], ii) adhesively bonded hybrid composite/metal joints [89,91,103,107], iii) adhesively bonded composite repair patches [95,102], and iv) welded thermoplastic composite joints [94,105]. Table 1 summarizes the main features, advantages, and disadvantages of FOSs for composite joints. Due to their small size, they are usually embedded in the composite adherends (under top layer), at the adherend/adhesive layer interface, or in the bond line. They have been shown suitable to monitor strain changes at the interface, disbond initiation, crack growth, and disbond length. Optical fibers are typically made of glass or polymer, which can transmit light over large distances. FBG is among the most popular sensor type for SHM of composite structures and joints. Bragg gratings are etched micro-structures inside an optical fiber core, reflecting a specific light wavelength [190]. When an FBG sensor is subjected to an external load (mechanical or thermal), the wavelength changes, allowing accurate strain measurements. A series of FBG sensors can be present along the length of the same optical fiber, leading to simultaneous strain readings at several locations.

More recently, Yashiro et al. [25] studied adhesively bonded CFRP double-lap joints under cyclic loading. They embedded three FBG sensors in the top 0° layer of the adherends and created a known disbond length (2 mm-long) to insure crack initiation under the sensors. They proposed an approach using the reflection spectrum and peak intensity ratio to estimate the disbond length. The high sensitivity of FBGs to non-uniform strain distribution suggests they are suitable for early assessment of moving disbond tip, compared to ultrasonic C-scan testing (see Fig. 8). Zeng et al. [26] embedded FBG sensors at the skin-core interface of sandwich composite L-joints subjected to bending load. They compared strain measurements with traditional resistance strain gauges mounted on the outer surface, and with finite element (FE) simulations. Embedded FBG sensors could adequately detect internal damage-induced strain changes (damage initiation, accumulation, and propagation), while outer strain gauges were insensitive to internal damage. However, given the curved interface, the reflection spectrum was too complex to detect wavelengths and therefore, the full spectral signal was a better option to measure strain.

Young et al. [107] monitored internal strain and stress development in dissimilar CF sheet molded composite/aluminum adhesive joints during manufacturing and post-processing (i.e., painting process). A sensing system based on high-definition FOS embedded at the bonded interface was used. Spatially resolved strain, residual strain, and thermal expansion over bond length for two types of adhesives were successfully measured. The collected data could allow prediction of localized strains, as well as their variation with time, temperature, and applied mechanical load. Rito et al. [102] used chirped FBG sensors for SHM of adhesively bonded patch repairs for GFRP panels. The sensor was embedded between the patch and the parent laminate, and the assembly was subjected to quasi-static and cyclic four-point bending tests. Damage progression (disbond from patch edges) was observed in the reflected spectra at the low wavelength end of the sensor, in the form of a dip or peak shift. No significant changes were seen at the high wavelength end. Therefore, it was recommended to use two chirped FBG sensors with their low wavelength end adjacent to the repair patch to monitor damage development.

Shohag et al. [104] used in-situ triboluminescent optical fiber (ITOF) sensors, combining the triboluminescence (TL) property of manganese-doped zinc sulfide. Polymer optical fibers were coated with a TL composite film by dip-coating, then incorporated into GFRP adhesive joints in double cantilever beam (DCB) and 3PB end-notched flexure (ENF) configurations. During DCB tests, ITOF sensor intensity increased at crack onset propagation and with mode I fracture toughness. During ENF tests, TL intensity changes were observed in the plastic deformation phase and during the failure phase. However, further research needs to address development of a damage index for TL-based detection as the level of damage cannot yet be determined.

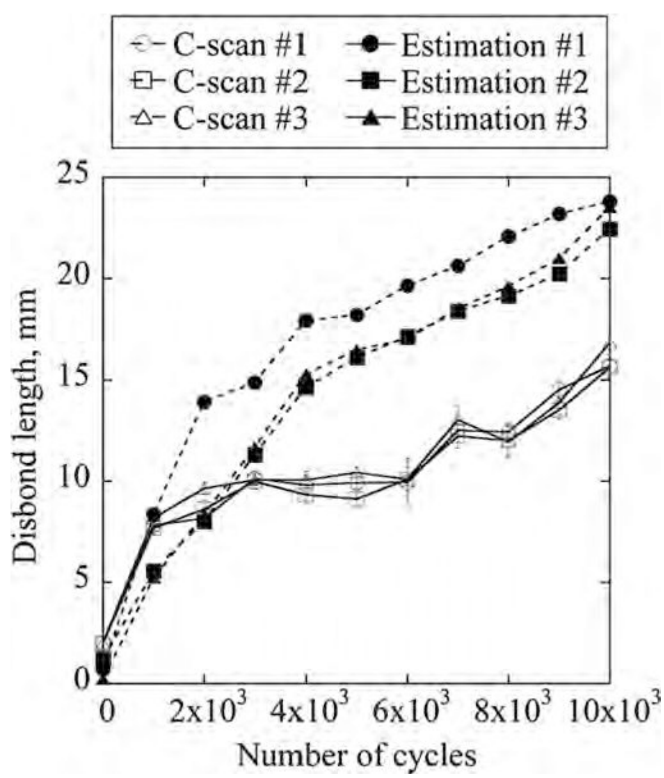

Fig. 8. Comparison of the disbond length evaluated by ultrasonic C-scan technique with the one estimated from the measured reflection spectra. Error bars represent the error range caused by the thickness of the band of white color tone in the C-scan images (Reproduced with permission from [25]).

There is very limited work in the literature on SHM of welded thermoplastic composite joints with FOSs. Notably, Wada et al. [105] embedded FBG sensors in ultrasonically welded single lap CFRP joints to evaluate the effect of welding process and applied tensile loads. Using optical frequency domain reflectometry, they measured residual strains after embedding, strain release after welding, and strain distribution during tensile loading application. This suggested potential of FBG sensors for weld quality monitoring and increased understanding of mechanical performance. Guo at al. [94] employed FOSs to monitor temperature profiles under different induction welding parameters for CF thermoplastic composite single-lap joints. The fibers were looped on the surface of the adherends and at the bond line, producing a larger number of data points than thermocouples, and illustrated through temperature matrices. They however did not perform damage monitoring under loading using the embedded FOSs.

While FOSs embedded in the bond line can monitor damage initiation and progression at the interface, one potential downside is their effect on the mechanical performance of joints. It is generally understood that embedding FOS in composite laminates does not significantly influence their mechanical properties, but there is limited literature on this topic for composite joints [90,93]. Recently, Grundmann et al. [93] embedded optical fibers with different coatings (polyimide and acrylate) and diameters (between 54 and 145 μm) and studied their effect on bond thickness and shear strength for CFRP single lap adhesive joints. Only polyimide-coated fibers with diameters below 100 μm showed no significant effect on quasi-static tensile shear strength. Overall, for the tested structural adhesives and composite adherends, polyimide-coated 80 μm optical fibers were identified as most suitable while maintaining SHM functionality.

3.2. Piezoelectric-based monitoring

While some studies experimentally tested the use of embedded piezoelectric micro-sensors in adhesive joints with metallic adherends [109,191], others employed them as part of external monitoring systems (transducer and/or sensor), as will be summarized in Section 4.6. Dugnani et al. [108,191] implemented piezoelectric sensors into aluminum single lap adhesive joints and developed an electromechanical impedance (EMI) approach to monitor the bond's integrity by measuring the dynamic response of the joint, under tensile loading, resulting from the presence of defects. This method was further refined by Zhuang et al. [109] for the same joint configuration and adherend type but intended for CFRP joints in aerospace applications. They proposed an EMI-based approach to detect weak bonds (i.e., "kissing" bonds), a type of defect that is particularly difficult to identify through typical acoustic or ultrasonic techniques. The 0.25 mm-thick sensors with a 3.1 mm diameter were embedded into three to four adhesive layers, with a total bondline thickness approximately equal to 0.45 mm. A damage index was defined as the root mean square deviation (RMSD), describing the average impedance change with the baseline, unloaded specimen. It was seen that this damage index remained generally unchanged but increased significantly when the joint was subjected to 80 % – 90 % of its failure stress. The state of the joint (healthy or degraded) can then be predicted according to a damage index threshold, indicating failure is eminent. As observed in Fig. 9, the location of the micro-sensors, in the middle of the joint or near the edges, was observed to affect the EMI response, suggesting they can predict failure initiation at an earlier stage. While the particular sensors used in this study did not affect mechanical

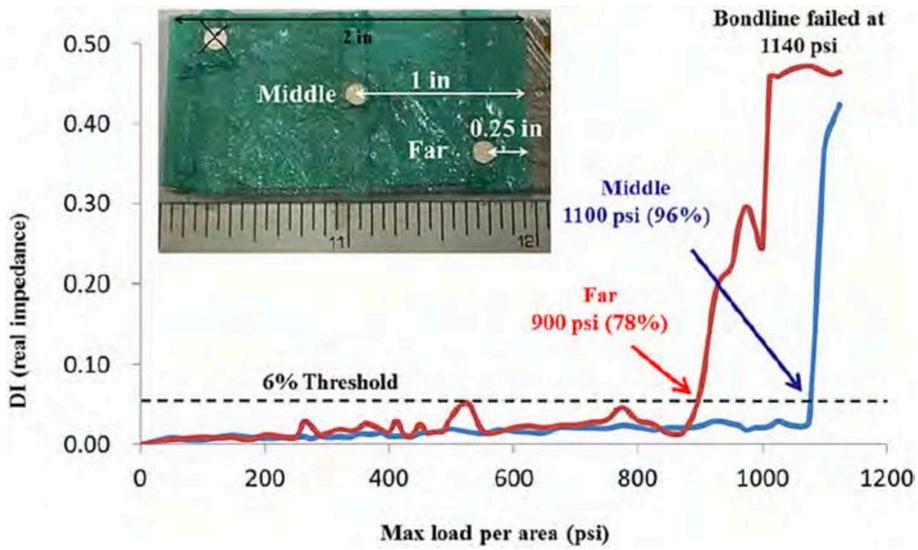

Fig. 9. Representative bondline degradation monitoring results with multiple piezoelectric sensors. The sensor on the edge is more sensitive to bondline degradation than the sensor in the middle (Reproduced with permission from [109]).

performance of the single lap joints, several of them would be required in practice to monitor large structures, which may have an effect on structural integrity. Moreover, incorporation of such sensors at the interface for other types of adhesives or fusion bonding methods may influence mechanical properties.

Deligianni et al. [14] used a different approach by incorporating PZT (lead zirconate titanate) particles in epoxy adhesives to create thick-film sensors intended for adhesively bonded joints. The sensors were however only tested on metal strips subjected to cyclic bending loads (four-point bending), not embedded into composite joints, but showed potential for strain monitoring.

3.3. Other embedded sensing methods

Other embedded sensing methods for composite joints include through-thickness Z-pins or tufting for adhesive bonding and eddy current (EC) array sensing films for bolted composite laminates [110,111]. Kadlec et al. [110] used Z-pins embedded in adhesively bonded CFRP adherends to assess crack-arresting mechanisms combined with a structural health monitoring method based on electrical resistance of the Z-pins. Cracked lap shear specimens (CLS) with embedded Z-pins were tested under tensile loading. Crack growth was monitored through visual observations and ultrasonic A-scans by stopping the tests at selected loading intervals. At the same intervals, the electrical resistance of the Z-pins was measured individually with a multimeter. It was shown that the normalized pin resistance increased with crack length (Fig. 10), indicating potential for localized SHM. This system needs to be further developed for real-time, simultaneous monitoring of several Z-pins resistance. Large-scale monitoring would require embedding Z-pins at different locations, which could influence mechanical performance.

Liu et al. [111] investigated the use of EC array sensing films directly bonded to bolts in mechanically fastened CFRP joints (14 mm diameter

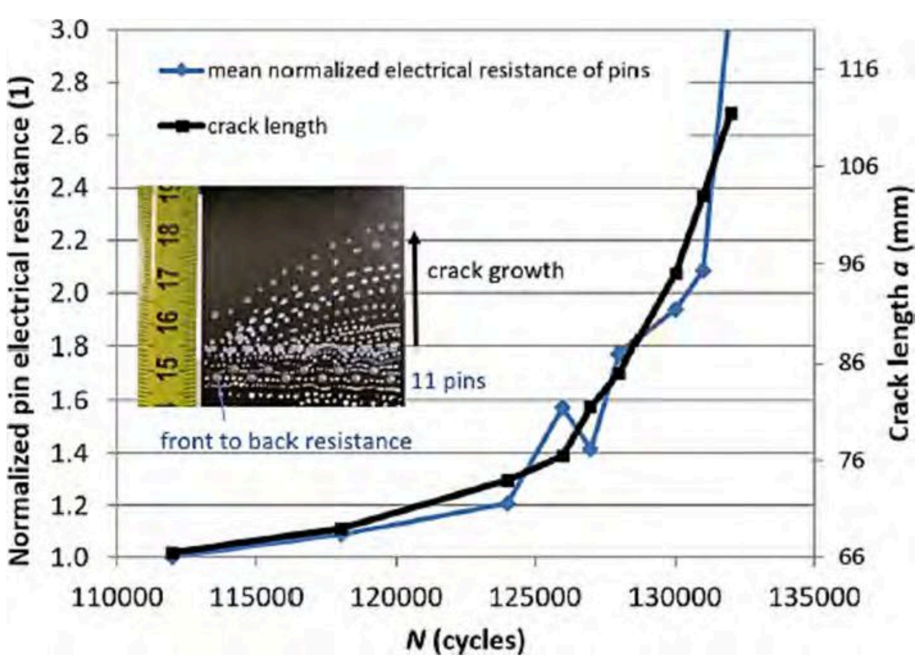

Fig. 10. Comparison of mean normalized electrical resistance of the Z-pins and fatigue crack length (α) for test specimen (Reproduced with permission from [110]).

holes). They consisted of an exciting coil and four sensing coils. Artificial cracks were introduced in laminates along two directions: i) radial direction from 0 to 4 mm crack length and ii) axial direction from 0 to 20 mm crack depth. For those cases, the induced voltage was measured and seen to generally increase with crack length, showing potential for crack growth monitoring. However, induced voltage in the radial direction past the 3 mm crack length remained constant, indicating a drawback with this sensing technology as eddy current had a limited penetration depth. Furthermore, future work should address real-time testing under mechanical loading and discuss challenges regarding implementation into real applications.

4. External monitoring techniques

In this paper, a damage monitoring technique that is not embedded at the interface or bond line of a joint is defined as "external" or "extrinsic". The following sub-sections will summarize current trends in main external monitoring methods for composite joints, including acoustic emission (AE), guided waves, structural vibrations and acoustics, laser shock adhesion test (LASAT), ultrasonic NDT, and other techniques such as piezoelectric sensors, thermography, and digital image correlation (DIC).

4.1. Acoustic emission

The acoustic emission method has been extensively studied for SHM of composite laminates and structures, but its application to composite joints is more limited. It is a passive method that can detect (i.e., "listen to") elastic energy propagating from any defect, pinpoint damage initiation and localization, and identify damage modes (e.g., cohesive or adhesive failure, etc.). One challenge with this method is that extensive analysis must be performed to correctly interpret acquired AE data, for which machine learning approaches have shown promise. For composite joints, AE was used for single-lap adhesive joints [117,118,124,125], finger joints [128], double-lap adhesive joints [119,123], joint adhesion in peel and double cantilever beam (DCB) tests [121], adhesively bonded panel/stringers [120,122], single-lap bolted joints [126], and adhesively bonded repair patches [74,113–116].

Weak bonds (or "kissing bonds") in adhesive joints, typically resulting from improper surface preparation or partially cured adhesives, cannot be reliably detected through traditional NDTs such as ultrasonic C-scanning. Teixeira de Freitas et al. [121] first studied the use of AE for detection of weak bonds in adhesively bonded CFRP through peel and DCB tests. They investigated the effect of surface treatments (including contaminated areas to simulate weak bonds) on cumulative number of hits and energy, related to failure modes (cohesive or adhesive). For instance, in DCB tests, AE showed no activity over the length of the weak bond (contaminated area), as shown in Fig. 11a. Overall, they observed that released energy for cohesive failure was higher than for adhesive failure mode and demonstrated the potential for AE to effectively detect weak bonds.

Saeedifar et al. characterized damage in metal-to-composite

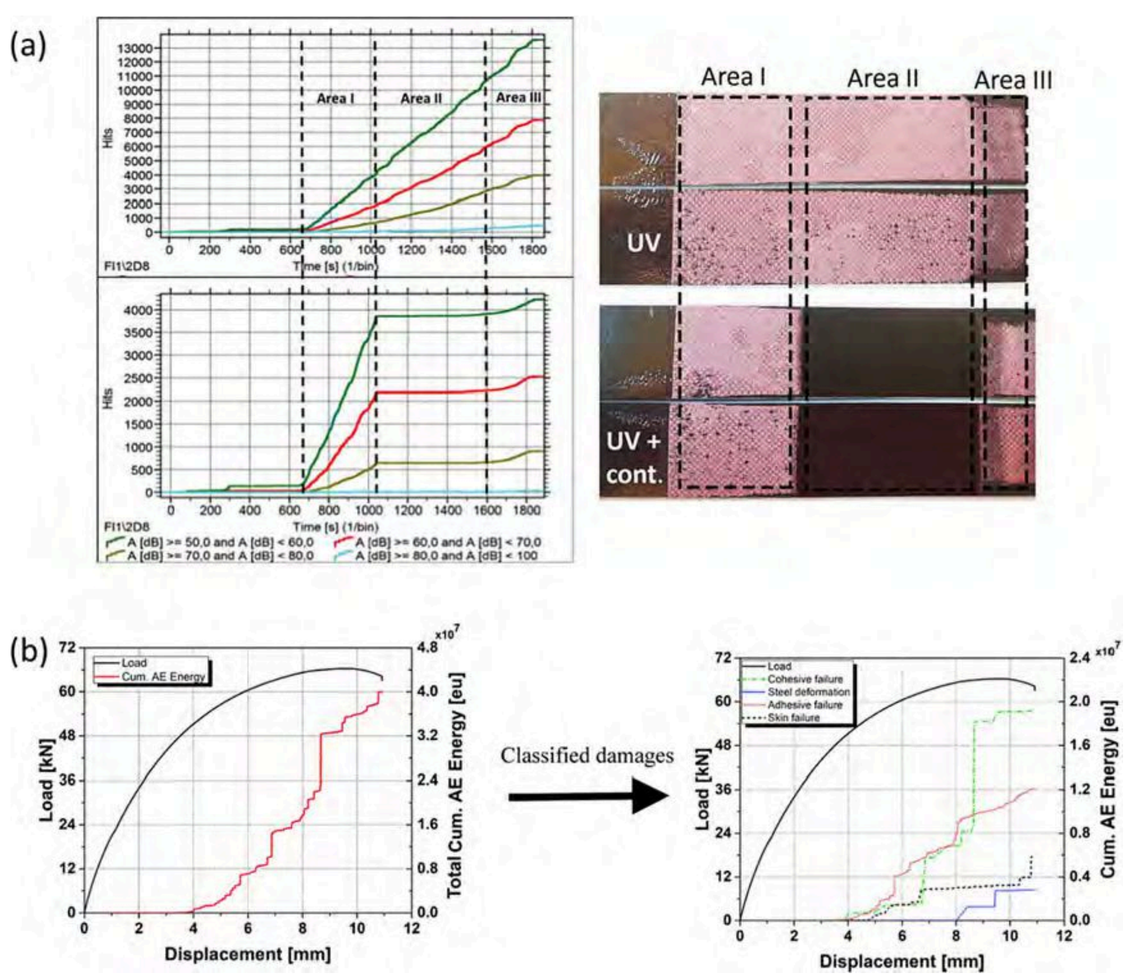

Fig. 11. (a) Cumulative number of hits during the peel tests for CF/epoxy specimens without (top) and with (bottom) contamination (Reproduced with permission from [121]) and (b) total cumulative AE energy and cumulative AE energy curve with classified damage modes for MMA-based DLJ specimens (CFRP adherends and MMA adhesive) (Reproduced with permission from [119]).

adhesively bonded structures through AE: steel-to-CFRP double-lap joints [119] and titanium panel to CFRP omega stringers [120]. For double-lap joints, adherends were tested individually under tensile loading to identify their damage mechanisms and corresponding AE features. An ensemble decision tree model was trained to classify damage types. For two adhesive formulations (methacrylate and epoxy-based), different damage modes were captured through AE, such as cohesive and adhesive failures (see Fig. 11b for methacrylate adhesive). The titanium panel bonded to CFRP stringers was tested under cyclic compression until failure. It was seen that AE could reliably capture damage initiation, its location, and its progression. AE features were clustered through particle swarm optimization to detect damage types. Results were favorably compared to digital image correlation (DIC) and showed better accuracy for damage onset detection.

Xu et al. [123,124] further explored machine learning approaches to identify damage modes from AE signals in adhesively bonded single-lap joints (SLJ) and double-lap joints. They employed an unsupervised clustering method by Fast Search and Find of Density Peaks (CFSFDP) through similarities between AE signals and features selection, such as rise time, AE counts, energy, time of duration, and peak amplitude. Various clusters corresponding to matrix cracking, shear adhesive failure, fiber/matrix interface debonding, delamination, and fiber breakage were created based on dB ranges. For all clustering methods and hyperparameters investigated, shear failure of the adhesive layer was found to be distinctive based on the selected AE features, when compared to different damage and failure modes in the adherends. Moreover, Xu et al. used clustering, time-domain, and frequency-domain analyses to study the effect of hygrothermal aging on damage behavior of SLJs. It was observed that aging reduced the AE peak amplitude for two damage modes, i.e., matrix cracking and fiber/matrix debonding. Generally, the ranges of peak amplitude and frequency band corresponding to shear adhesive failure were 40 to 50 dB and 40 to 45 kHz, respectively. Overall, AE shows potential for damage initiation detection, location, and progression, as well as damage mechanisms identification through clustering methods for single-lap or double-lap joints.

Contact conditions in single-lap bolted composite joints under flexural vibrations and fatigue loading were characterized using intrinsic mode functions of AE signals by Zhang et al. [126]. The effect of torque applied to the bolted joints on cumulative energy (Fig. 12a) and AE signals amplitude (Fig. 12b) was studied. It was observed that at low torque values ($\leq$ 3 N·m), changes in the energy release rate were more significant than at higher torques ($\geq$ 7 N·m), indicating less stable contact conditions under this torque. Tightening conditions and vibration-induced loosening of the joints could be detected within 4 to 7 N·m torque range.

Andrew et al. [113–116] investigated the use of AE for damage characterization in adhesively bonded repair patches on GF/epoxy laminates under different load cases: bending, compression, and tension. The mechanical response of repaired laminates with homogeneous and hybrid patches was compared. For all load cases, cumulative counts and events location were recorded to evaluate damage onset, location, and type (matrix cracking, fiber/matrix debonding, and fiber breakage). Damage was generally observed over the patch area or the whole repaired laminate, but this AE monitoring approach could not directly discriminate between patch/laminate matrix cracking and adhesive damage (adhesive or cohesive failure between patch and parent laminate).

4.2. Guided waves

Guided wave-based SHM methods are promising because they are inexpensive, easy to implement into existing structures (with lightweight transducers), possess large scanning areas, and are not affected by ambient vibrations [192]. However, correct implementation and data analysis for damage localization, type, and severity tend to be complex. Various wave forms have been investigated for SHM, but the most common one for composite structures is the Lamb wave because it propagates through shell-like components (i.e., thin plate laminates). In the literature, guided waves have been explored for different types of composite joints, such as adhesively bonded SLJs [96], bonded skin/stringer assemblies [7,133,140–142,146], bonded T-joints [136], bonded repair patches [129,134,138,147], bolted joints [132,144], and ultrasonically welded thermoplastic composite joints [48,137].

Karpenko et al. [96] monitored fatigue damage in adhesively bonded GFRP SLJs with guided waves and FBG sensors. FBG sensors embedded in the bond line and on adherends were used to measure damage progression. Guided waves time-of-flight (ToF) of the fundamental modes, collected in pitch-catch mode, monitored yielding of the adhesive bond line. As guided waves are sensitive to geometric changes (such as deformation of adhesive layer and adherends), they can provide a more complete assessment of fatigue damage than FBG sensors. Sherafat et al. [141,142] used Lamb waves to monitor the quality of bonded skin-stringer structures (Fig. 13a). CFRP panels were joined to stringers with undamaged and damaged adhesive bonds. The in-plane and out-of-plane velocity was measured with a 3D Laser Doppler Vibrometer for several points in a circular grid. The guided waves behavior in reflection, transmission, and scattering were investigated with respect to anti-symmetric (A0) and symmetric (S0) modes, frequency, excitation angle, and joint quality. Wave scattering at the disbonded area under S0 mode was most promising below 350 kHz, showing 60 % increase in the scattered field. This resulted in a modified radiation pattern for the bond, illustrated in Fig. 13b. Overall, patterns amplitude and direction were influenced by the presence of damage at the interface, suggesting SHM guidelines for reliable damage identification. Yu at al. [7,146]

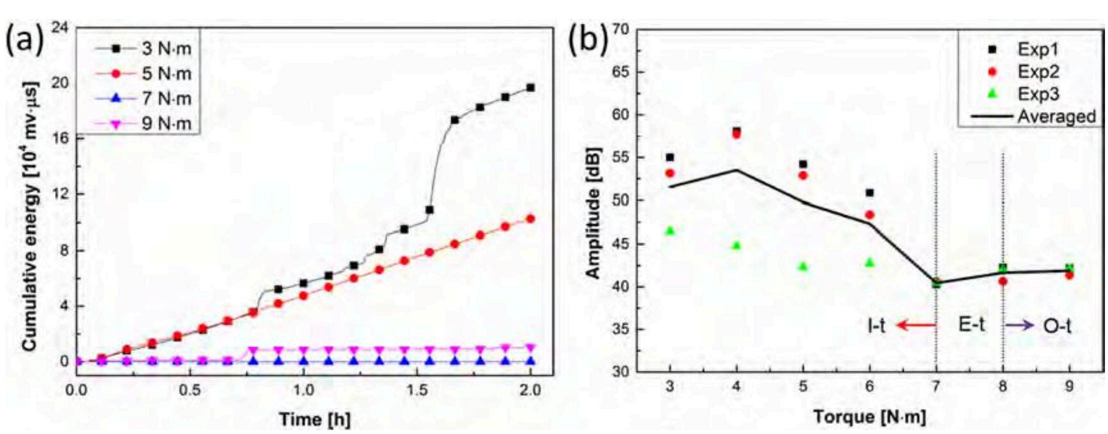

Fig. 12. (a) Cumulative energy of the AE signals captured from single-lap bolted joints under fatigue and (b) averaged amplitude of the AE signals captured from three bolted joints under different torques (I-t: insufficiently tightened, E-t: efficiently tightened, and O-t: over-tightened) (Reproduced with permission from [126]).

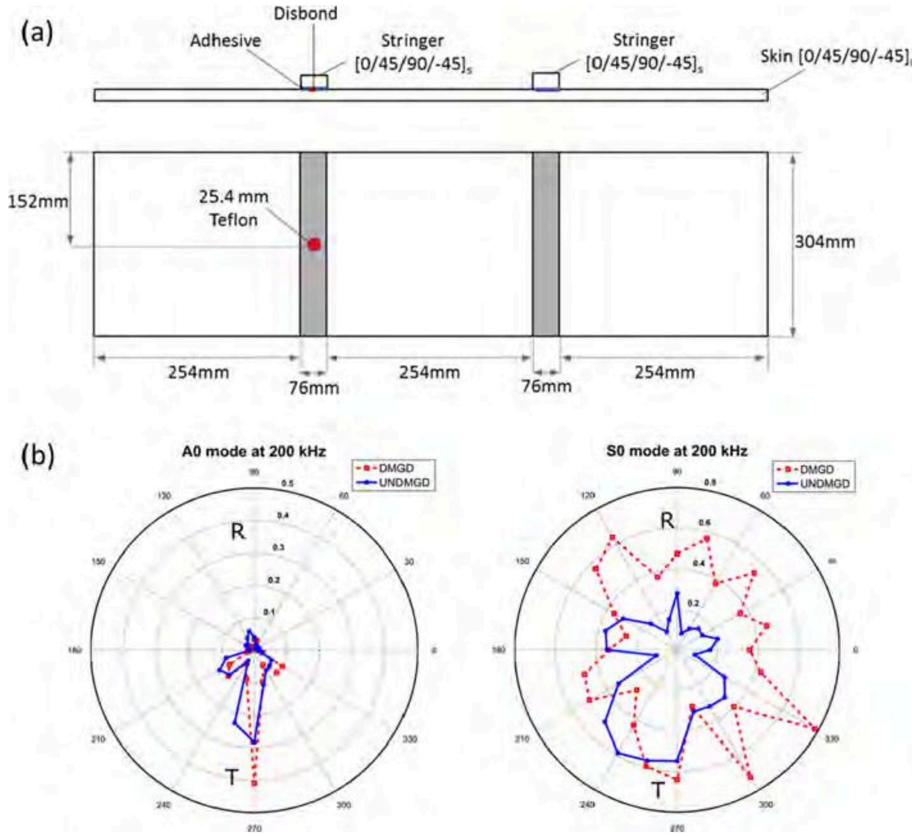

Fig. 13. (a) Schematic view of skin-stringer bonded joint configuration: damaged (left) and undamaged (right) joints and (b) effect of excitation frequency and propagating mode on the scattering behavior: diffraction pattern of A0 (left) and S0 modes (right) for the undamaged (solid blue) and damaged (dashed red) joints at 200 kHz (Reproduced with permission from [141]).

studied the structural integrity of adhesively bonded Al stiffener/CFRP composite skin assemblies through a feature guided wave (FGW) approach using finite element analysis and experiments. FGWs are well-suited for rapid inspection of long-range damage features by positioning an array of sensors, e.g., placed on the composite skin close to the bond line. A notch defect was inserted in the adhesive, which resulted in strong diffracted waves captured by the nearby sensors. An imaging technique (synthetic focusing algorithm) was employed to convert the signals into enhanced intensity, providing information about defects location and severity. This technique may be combined with traditional guided wave systems to offer a more complete overview of the structural condition of the entire structure.

Ochoa et al. [48,137] were the first ones to use ultrasonic guided waves to investigate the presence of manufacturing-induced defects and the effect of welding parameters (i.e., bond line thickness) for ultrasonically welded thermoplastic composite (CF/PPS) joints. To produce defects at the weld line, triangular protrusions (also called “energy directors”) were integrated on the bottom adherend and partially melted during the welding process, thereby creating two defective scenarios: i) unwelded areas with interspersed welded zones and ii) fiber bundles distortion. ToF and characteristic frequency analyses were combined to differentiate between those two defect types, for which accuracy varied from 60 % to 100 %, respectively. Regarding the effect of bond line thickness (controlled during the welding process), the correlation coefficient indicated signal shape differences resulting from variations at the welded interface, such as bond line thickness and intermolecular diffusion.

Core-junction thickness and joint disbonds in sandwich composite panels (GFRP sheets bonded to honeycomb core) were theoretically, numerically, and experimentally analyzed with Lamb wave propagation by Sikdar and Ostachowicz [143]. A0 mode amplitude increased with joint-debond length (Fig. 14a) and debond localization was identified through an imaging algorithm using the Hilbert-transform of the signals and the debond-index (Di) magnitudes over the panel surface area (Fig. 14b).

Lamb waves were also used for SHM of mechanically fastened GF/epoxy joints under tensile load by Yang et al. [144]. The effect of pre-tightening torque and tensile load on guided wave signals was investigated for single bolt and double bolt specimens. Results indicated that S0 and A0 modes amplitudes decreased with increasing torque and load, suggesting S0/A0 amplitude difference could be employed for failure identification, although no clear guidelines between net tension, shear out, and bearing failures are presented.

In the literature, several hybrid SHM systems were used alongside guided waves (i.e., combination of more than one monitoring technique). For instance, Lambinet et al. [134] studied bonded repair patches on impacted CFRP panels and carried out electromechanical impedance (EMI) and Lamb wave analyses. Damage was effectively detected in repaired panels after impact, but the localization accuracy was lower in comparison to undamaged laminates because of reflections coming from the patch boundaries. Bond line quality was monitored during tensile fatigue loading at specific intervals. The Damage Index (DI), calculated from the root mean square deviation (RMSD) between baseline and fatigue interval signals, was used to detect damage. The DI values increased with load and number of cycles, showing a progression in three phases. Ma et al. [136] employed Lamb wave (with nine PZT sensors), high-speed camera, and FBG sensors to detect interface debond in CFRP T-joints. Guided waves characteristic parameters, such as the peak-to-peak amplitude of the direct wave (Vpp) and total wave energy, were extracted, then compared to center wavelength of FBG and load–displacement curves during tensile tests (Fig. 14c). The characteristic parameters were found to be in good agreement with FBG

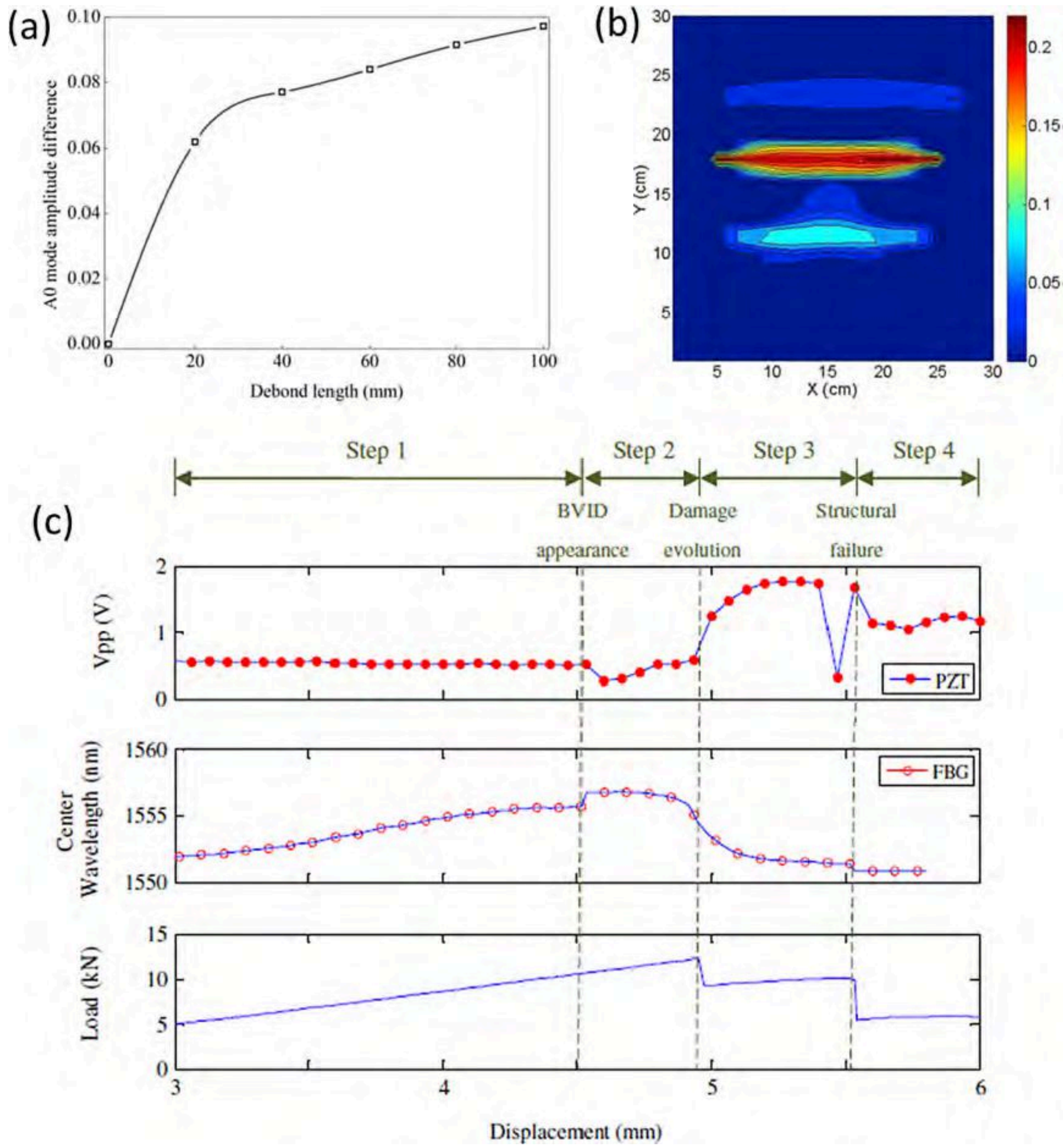

Fig. 14. (a) Influence of joint debond length on A0 mode amplitude difference for undamaged and damage-affected signals, (b) debond-index (Di)-map in contour pattern showing the joint-debond location in the panel (Reproduced with permission from [143]), and (c) comparison between PZT sensors (guided wave) center wavelength of FBG sensor and tensile load with respect to tensile displacement (Reproduced with permission from [136]).

sensors, load–displacement curves, and high-speed camera, and captured damage evolution (including initiation) and structural failure earlier than other methods.

4.3. Structural vibrations and acoustics

Low-frequency structural vibration-based approaches are attracting interest of researchers for damage identification [193], but there are still limited studies on fiber-reinforced polymer joints. Successful application was demonstrated for single lap metal-composite adhesive joints, skin-stiffener joints, and single lap bolted joints [148–153]. Those approaches may be classified based on their damage features in the time domain, frequency domain, or modal domain (mode shape curvatures, natural frequencies, or mode shapes). Medeiros et al. [148] investigated the debonding in bi-clamped adhesively bonded titanium-CFRP joints through structural vibrations, which compared the Frequency Response Functions (FRFs) of three case studies: i) identifying the effect of piezoelectric transducer (PZT sensor) on FRFs, ii) assessing the effect of artificial defect (Teflon layer) using accelerometers, and iii) damage monitoring via PZT. Mickens' damage metric and modified Mickens' damage metric, comparing the magnitudes and phase angles of FRFs for undamaged and damaged samples, were employed within a frequency range of 50 to 350 Hz. Representative results of the computational model are displayed in Fig. 15a. The results indicated that PZT (attached to the titanium) led to a reduction in natural frequencies at higher frequencies (> 200 Hz), pre-debonding damage also shifted natural frequencies to smaller values, but more significantly than PZT, and both metrics provided potential for SHM applications.

The vibro-acoustic modulation (VAM) approach was extended to composite-composite joints. For instance, single lap CFRP bolted joints were monitored using VAM for bolt loosening subjected to a low-frequency vibration (pump excitation) of 758 Hz and a high-frequency acoustic wave (carrier excitation) of 14.89 kHz [153]. Both numerical and experimental results showed an increase in sideband magnitudes, quantitatively related to bolt loosening, with the decrease of residual torque. An illustration of sideband magnitudes is shown in Fig. 15b. The

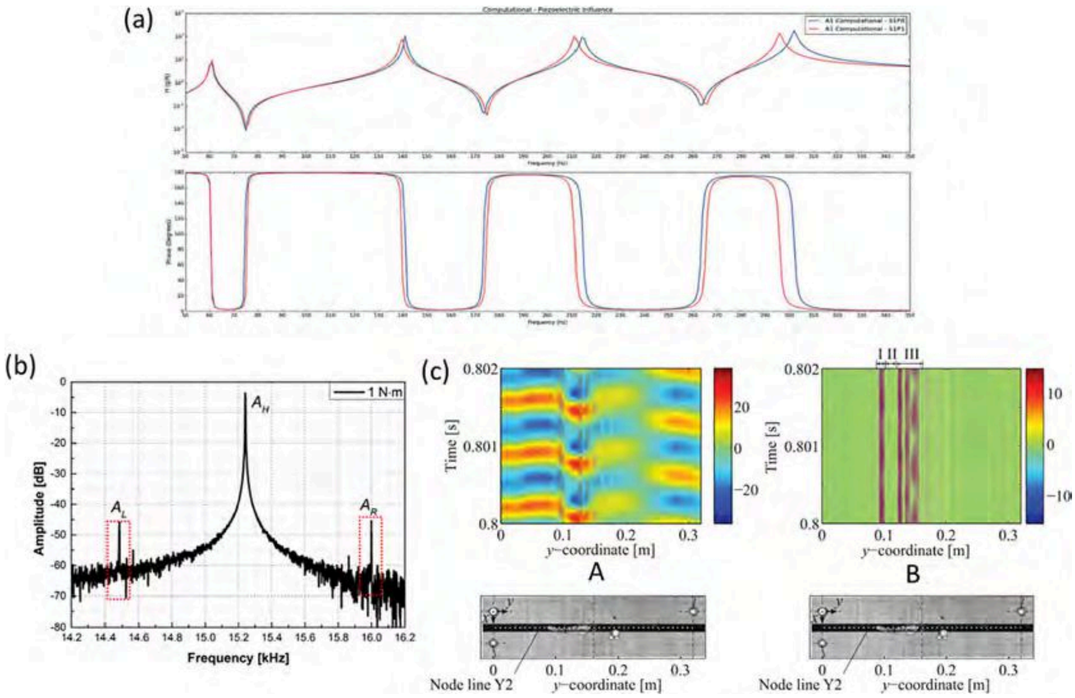

Fig. 15. (a) Computational results of specimen S1P0 (without damage/without PZT sensor) and S1P1 (without damage/with PZT sensor) (Reproduced with permission from [148]), (b) Experimental sideband response of the CFRP bolted joints under bolt torque of 1 N·m (A_L: magnitude of actual left sideband, A_H: magnitude of probing wave at f_H, and A_R: magnitude of actual right sideband) (Reproduced with permission from [153]), and (c) original (A) and bandpass filtered (B) (40–60 kHz) velocity response measured at node line "Y2" of damaged structure (Reproduced with permission from [150]).

authors also proved that the VAM-based method had a higher sensitivity to bolt loosening compared to an elastic wave-based linear approach. In addition, the VAM approach was employed to monitor complex bonded structures, such as skin-stiffener. In [150], impact damage between CF/PEKK skin and stiffener was identified via the modulation of carrier excitation by pump excitation. During the test, velocity response was captured and then decomposed through bandpass filter and Hilbert transform to get instantaneous amplitude/frequency of carrier, their changes corresponding to the damage in composite structures. As depicted in Fig. 15c, the locally high amplitude modulation in region I and III clearly demonstrated the presence, location, and even the length of damage in skin-stiffener joints, which shows the potential of VAM for damage identification. In [152], the same group also demonstrated the use of mode shape curvature changes and modal strain energy damage index to identify defects in skin-stiffener joints. They however point out that the design of the structure and defect position influence the effectiveness of this SHM method.

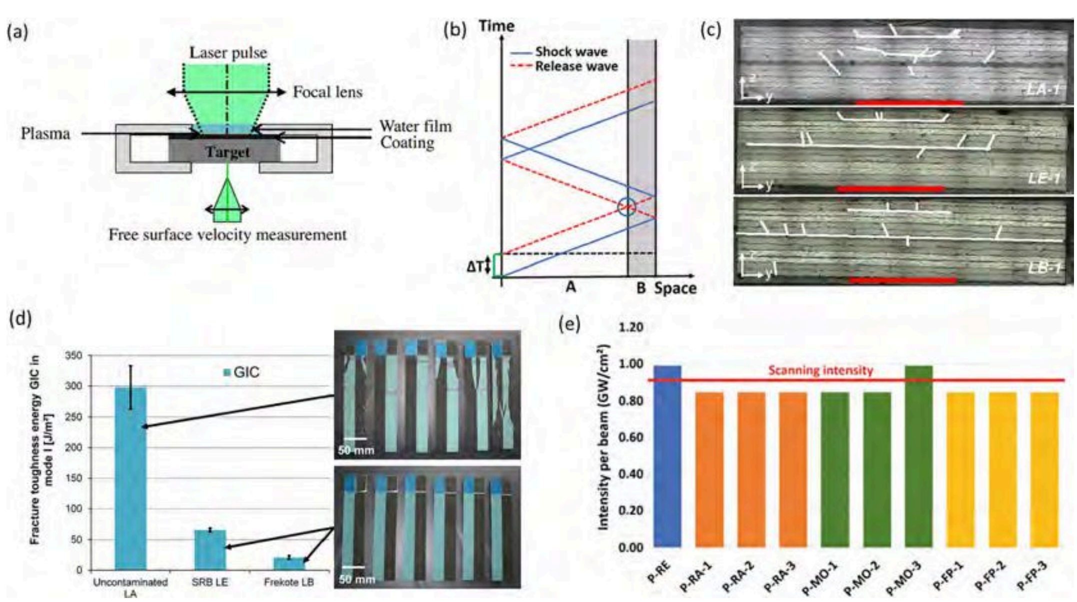

Fig. 16. (a) Sketch of laser shock adhesion test method (Reproduced with permission from [196]), (b) time–space diagram showing the behavior of shock waves within the sample [154], (c) cross-section of reference (LA) and two weak bond samples (LE and LB) (Reproduced with permission from [155]), (d) fracture toughness energy of LA, LE, and LB samples (fracture surface in insert) (Reproduced with permission from [155]), and (e) LASAT results of uncontaminated and contaminated samples [154].

4.4. Laser shock adhesion test (LASAT)

LASAT is a technique to evaluate the quality of an adhesive bondline. This approach generates shocks using a high-power laser. As illustrated in Fig. 16a, when laser beam is focused on the target surface via focal lens, the irradiated surface is rapidly transformed into a dense plasma, which is confined using water to increase the pressure, allowing more compact lasers to be used. Subsequently, shock waves are created by the expansion of plasma and propagate through the sample. When reaching the sample back-face, the shock waves are reflected as release waves. They fold back and cross with the incident release waves, resulting in locally high tensile stress, circled in Fig. 16b. As a result, corresponding damage may occur if the tensile stress exceeds the bonding threshold.

LASAT was first introduced by Vossen [194] to measure the bond strength of film-substrates. In the past decade, this NDT method has been further developed for bonded composites [154–159,195,196]. For example, Ehrhart et al. [155] evaluated adhesion strength of uncontaminated and contaminated CFRP joints by two types of release agents (noted LB and LE). Under the same highest intensity laser shock level (~2.3 GW/cm^2), only transverse cracks and delamination occurred without any debonding in uncontaminated composite joints compared to the two contaminated cases, as shown in Fig. 16c. This outcome demonstrated the feasibility of LASAT to discriminate adhesion quality. In addition, the observations for both types of contaminated samples showed good agreement, indicating a similar adhesion level identified by double cantilever beam test in Fig. 16d. However, in this technique, the highest tensile stress cannot be optimally located when the interface is far away from the back of the sample. Subsequently, Sagnard et al. [159] developed symmetrical LASAT, which generated shock waves on both sides of the sample, with the highest tensile stress occurring at the intersection of the two reflected shock waves. Moreover, this location can be shifted through time delay. As a result, the limitation of single LASAT was overcome. More recently, a book [154] summarized LASAT used to assess adhesive bonding of CFRP. Samples were subjected to increasing laser intensity and ultrasound scanning was used to determine whether the bond had failed. If it failed, that energy was assumed to be the bonding threshold, whereas if not, the energy was increased. If the obtained threshold was lower than the standard value from the reference sample, it indicated that LASAT successfully detected the problematic samples. A representative example is clearly depicted in Fig. 16e, where the height of each bar represents the amount of energy required to fracture the bond. Therefore, LASAT successfully discriminated eight out of nine release agent (RA), moisture (MO), and fingerprint (FP) contaminated samples. Nevertheless, the LASAT technique requires optimization since it can damage samples.

4.5. Ultrasonic NDT

Ultrasonic scanning is one of the most commonly used NDT techniques for evaluating the integrity of composite structures. In ultrasonic NDT, a wave propagating through the inspected media is reflected, transmitted, or scattered from the interface, which is received by a transducer. In general, the travelling speed and time of waves, as well as a series of obtained images, can be used to determine material quality and joint integrity. For example, the attenuation coefficient was used to distinguish between good and poor bonding in [166]. Amplitude images were captured to detect flaws in GFRP joints in [163]. Yashiro et al. [25] employed ultrasonic C-scanning technique to evaluate the disbond area (created by inserting a PTFE film) in adhesively bonded CFRP double-lap joints subjected to cyclic loading. Ultrasonic C-scan images in Fig. 17a-f showed that disbonds extended as the number of cycles increased. However, the initial disbonded area could not be detected before cyclic testing began, indicating that this conventional NDT technique was not suitable for detecting small disbonds like kissing bonds. In recent years, efforts have also been made in developing other new techniques in this field, such as pulse-echo immersion ultrasonic technique [165,166] and

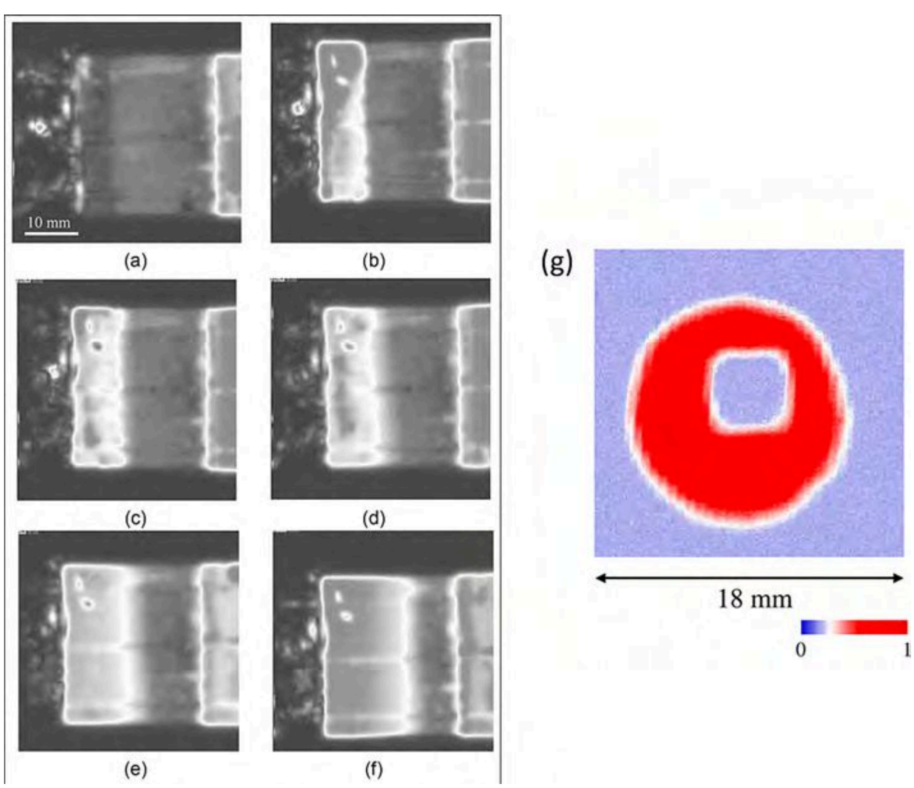

Fig. 17. Ultrasonic C-scan images observing crack extension in CFRP double-lap joints with initial disbond at: (a) N = 0, (b) N = 2000, (c) N = 4000, (d) N = 6000, (e) N = 8000, and (f) N = 10,000 (Reproduced with permission from [25]); (g) maximum amplitude images for a cross-ply CFRP/Al specimen with a 5 mm square disbond by transmitted ultrasonic wave (Reproduced with permission from [168]).

phased array ultrasonic testing [163,164,167].

Additionally, Toyama et al. [168] monitored disbonds in adhesively bonded CFRP/Al joints through pulsed laser scanning ultrasonic inspection technique. Firstly, a quick inspection was carried out in the entire bonded joint regions and 200-kHz low-frequency Lamb waves were visualized. Distinct phase delays, reflected waves, and high amplitudes were observed at the artificial disbonds (PTFE films), which confirmed defect location. In order to further determine the shape and size of disbonds, secondly, detailed inspection using laser ultrasonic transmission method with high frequencies (8 MHz) was performed in an area including a small disbond detected by the quick inspection. As the disbond between PTFE films and adhesive layer prevented the ultrasonic waves to propagate through, a slightly higher amplitude was generated along the disbond. Consequently, the shape of the defect was clearly imaged, and its size was easily measured (Fig. 17g).

Although ultrasonic NDT techniques have been widely used for inspecting joint integrity, they still face some challenges: i) high attenuation and low signal-to-noise ratio result from the inherent anisotropy and heterogeneity of composite materials, ii) difficult to detect zero volume interfacial disbonds, i.e., kissing bonds, for conventional ultrasonic techniques due to their transparency for ultrasonic waves, and iii) not readily capable of online, real-time monitoring. However, Brotherhood et al. [197] investigated the detectability of kissing bonds in Al-Al adhesive joints using conventional longitudinal wave and shear wave ultrasonic inspection and high power ultrasonic inspections through determining the reflection coefficient of imperfect bonds and comparing the non-linear behavior of disbonded interfaces, respectively. The experimental results indicated that high power techniques had the highest sensitivity only under low contact pressures, while longitudinal wave inspection showed better sensitivity subjected to high contact pressures and higher than shear wave throughout the whole testing process.

4.6. Other external monitoring techniques

Other external damage monitoring techniques include EMI (e.g., piezoelectric sensors placed outside bond line), thermography, and digital image correlation (DIC). While guided waves is a more common approach with external piezoelectric sensors for SHM of composite joints, EMI has also been investigated for SLJs [162] and bonded plates [160,161]. Malinowski et al. [161] showed that weak adhesive bonds could be detected with the root mean square index and conductance peak frequency change. Zhu et al. [162] used an EMI-based approach to monitor single lap CFRP adhesive joints under quasi-static tensile loading. They leveraged the root mean square deviation index of raw impedance signals and the effective structural mechanical impedance (ESMI) signatures. This monitoring technique showed that reduced data processing could effectively lead to evaluation of joints structural integrity. Some future work should however include higher strain rates and cyclic loading, and correlation with damage type.

Pulsed phase thermography (PPT), capable of rapidly imaging large areas, has been employed to monitor composite joints as well [169,170,172]. PPT applies a square pulse to the surface of a sample to heat it. Consequently, the temperature of the sample surface changes as the heat propagates along its thickness. If the performance of heat transfer below the surface is uniform, the displayed surface temperature will be uniform. On the contrary, if the surface temperature of the tested area is inconsistent, it indicates that the heat transfer performance of a certain part of the materials is different, and thus, this area is likely to contain defects. In PPT, phase contrast value, $\Delta\varphi$, is an important parameter in determining defects. Tighe et al. [171] studied the detectability of three artifical defects including polytetrafluoroethene (PTFE) insert, Frekote mould release agent, and silicon grease in adhesively bonded CFRP joints using PPT. They found that PTFE insert might not introduce a debond in adhesive joints (Fig. 18a), with an unchanging $\Delta\varphi$ under loads. In addition, Frekote release agent was not suitable for creating kissing defects either. Not only because it penerated into adhesive causing it to be removed from the bond region, but also, its low viscosity made it spread out to a large area. Unlike them, silicon grease was capable of similuating kissing defects. However, thses kissing bonds were undetecable using PPT when joints were unloaded due to its negligible influence on heat transfer without sufficient thermal contact. However, upon loading, defects opened, leading to a detectable $\Delta\varphi$, which is clearly illustrated in Fig. 18b with a significant increase of phase contrast subjected to loads. In this way, defects could be idendified effectively.

Another NDT method, digital image correlation (DIC), has been used to monitor kissing bonds. Kumar et al. [173] investigated the detectivity of dry contact kissing bonds in adhesively bonded single lap GFRP joints with different defect areas (25 %, 48 %, and 70 % kissing bond area) under different loads until failure, through DIC technique. A representative DIC strain field (ε_{yy}) for a 48 % kissing bond area is presented in Fig. 19, showing an obvious separation between kissing bonds and healthy area. Based on the strain field characteristics, the sizes of kissing bond defects were calculated with MATLAB. Finally, they proved that DIC was effective for detecting kissing bond defects under 50 % failure load. Furthermore, the failure load of joints decreased as the kissing defect area increased, especially when kissing bond area percentage was large (70 %). Aside from the aforementioned techniques, high-frequency dielectric measurements [174] and heterodyne effect [175] were also developed.

5. Conclusions

Although damage monitoring techniques for composite joints have attracted significant interest in the literature, they are facing several challenges for which future research is still needed. In the present work, substantial assessment of current approaches to address various aspects of damage detection for fiber-reinforced polymer joints (adhesive, mechanical, and welded) was summarized (see Table 1 for overview).

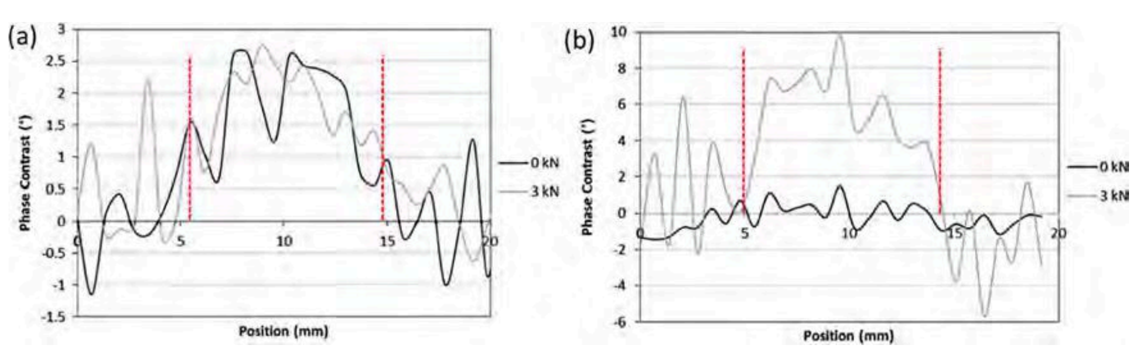

Fig. 18. PPT phase contrast data taken along the profile line across (a) PTFE insert and (b) silicon grease contamination for both the unloaded and 3 kN static loaded cases. Vertical dashed lines mark the extent of the defect (Reproduced with permission from [171]).

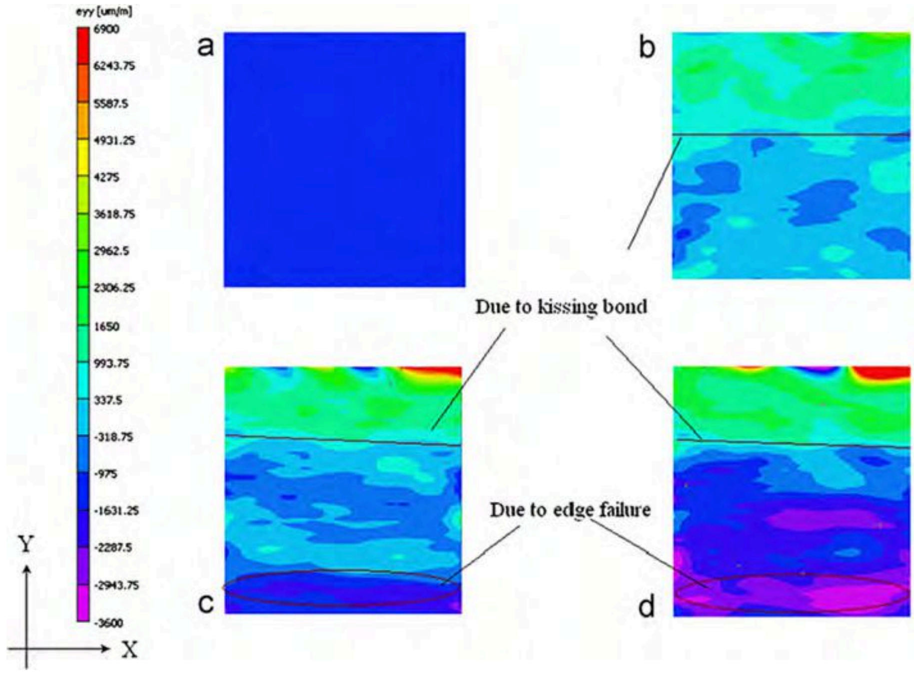

Fig. 19. DIC strain field (e_{yy}) images for a K48 adhesive joint (48 % kissing bond area). (a) No load, (b) 50 % of failure load, (c) 75 % of failure load, and (d) just before failure (Reproduced with permission from [173]).

Based on the above review, the following conclusions can be drawn, first for nanocomposite-based sensing:

- Nanoparticle concentration and dispersion have a significant effect on sensing sensitivity and may affect mechanical properties of composite joints (e.g., lap shear strength). The electrical resistance response, the most researched approach in nanocomposite-based sensing, is highly affected by nanofiller concentration, loading direction, and joint configuration, which are dominant in determining failure modes. However, so far, relating electrical resistance changes to specific failure modes and locations remains a challenge.
- Related research on welding technologies, such as resistance welding, induction welding, and ultrasonic welding, is mostly limited to heating element design, mechanical performance, welding parameters, and weld quality. Efforts toward development of damage monitoring methods for ultrasonically welded thermoplastic composite joints are recent, but there is an imminent need for further investigation encompassing a range of fusion bonding methods.

Second, for intrinsic sensing methods:

- Embedded FOSs are the most widely used sensors for SHM of composite joints. In addition to temperature changes, FOSs are capable of monitoring strain changes at the interface, disbond initiation, crack propagation, and disbond length. It is worth noting that mechanical properties of composite joints are susceptible to the embedded sensors in the bond line or at the interface. Moreover, systems and data analysis for damage type identification can be complex for large structures.

Finally, for external sensing methods, acoustic emission and guided waves are the most widely studied approaches for reliable, real-time damage monitoring:

- AE demonstrates relatively high reliability in detecting damage initiation, location, and progression, and distinguishes between different failure types. Furthermore, it has shown potential to monitor kissing bonds as well. However, data analysis is complex for automated damage classification, with recent advances leveraging machine learning algorithms.
- Guided waves have been employed for SHM of adhesive, bolted, and welded composite joints. The implementation of this method is complex, especially regarding sensor placement, and data analysis for damage localization, type, and severity is challenging.
- Structural vibration-based methods have shown potential for damage detection in adhesively bonded and bolted joints, including bolt loosening, location, and size. However, it is noted that this method's effectiveness depends on structure design and defect position.
- Ultrasonic NDT methods have been used in academia and industry for reliable damage detection, including defect location and size. However, it presents particular challenges for composite joints, especially for detection of weak bonds. Moreover, other methods, such as FOSs, have been shown to detect damage initiation more accurately than ultrasonic NDT.

5.1. Gap analysis and future research needs

By reviewing the existing publications, numerous techniques have been employed and improved to monitor damage in fiber-reinforced polymer joints, including considerations toward type, severity, and localization. However, there are still some issues to be addressed. Overall, SHM methods cannot quantify joints' mechanical properties, but some can relatively classify good versus weak bonds, more specifically for adhesive joints (e.g., AE, EMI). It is therefore expected that to obtain a complete overview of the damage state, more than one SHM technique should be combined, which remains a challenge for large and complex structures in industrial applications. Toward this end, machine learning approaches and the combination of multiple techniques is particularly important. In this respect, the fusion of different techniques, such as raw data fusion, feature-level fusion, decision-making-level fusion, etc., is a promising research direction. AE, guided waves, or structural vibration-based methods are attractive because they can be distributed on large, existing structures, but differentiating damage at the bond line or within laminates/adherends necessitates an extensive database encompassing all scenarios and corresponding signatures. It may be advantageous to incorporate additional sensors localized at the bond line, such as embedded nanocomposite films or FOSs. However, identification of damage sensitive features and classifiers toward high detection probability, while avoiding false warnings, remains an important challenge for SHM.

Some areas for improvement depend on joining technique. For instance, significant advances have been made in adhesively bonded joints, especially in detecting damage initiation and progression under load. On the other hand, welded composite joints have seen very little attention in the literature regarding their failure behavior and SHM. As weldable polymer composites (e.g., traditional thermoplastic, liquid thermoplastic vitrimer, or recyclable epoxy matrices) gain popularity in various industries due to their sustainability, there is a need for further research toward reliable SHM.

For nanocomposite-based sensing, correlation between electrical resistance changes, failure modes, damage type, and location within the joint requires more in-depth analysis leading to robust detection systems. This includes novel designs with controlled nanoparticles orientation and distribution, capturing behavior over the entire bond line. In addition, incorporating nanoparticles or embedding sensors at the bond line or at the adhesive/adherend interface, i.e., FOSs, may affect the mechanical performance of joints. Therefore, this field requires further study.

In general, damage detection of adhesively bonded, mechanically fastened, and welded joints subjected to static monotonic and cyclic tensile loading through various techniques has been well characterized. However, the failure behavior of composite joints under a combination of loading scenarios that consider operational and environmental variability (e.g., temperature, humidity, loading mode, and boundary conditions) has not been investigated in depth. While statistical techniques may compensate for this variability, increased confidence in such methods is needed, especially for joints.

Finally, experimental results have shown that embedded sensors and external non-destructive techniques can evaluate the structural health of composite joints, but there is limited research toward modeling approaches capable of predicting damage behavior and optimizing in-situ SHM techniques and their implementation, especially for nanocomposite-based sensing.

Declaration of Competing Interest

The authors declare that they have no known competing financial interests or personal relationships that could have appeared to influence the work reported in this paper.

Data availability

No data was used for the research described in the article.

Acknowledgements

This work was supported by the Louisiana Board of Regents under the Research Competitiveness Subprogram (contract number LEQSF (2018-2021)-RD-A-05); the LSU Graduate School Economic Development Assistantship; and the National Science Foundation CAREER award (CMMI, Advanced Manufacturing, Award #2045955).

References

[1] Li HCH, Herszberg I, Davis CE, Mouritz AP, Galea SC. Health monitoring of marine composite structural joints using fibre optic sensors. Compos Struct 2006;75(1–4):321–37.
[2] Li HCH, Herszberg I, Mouritz AP, Davis CE, Galea SC. Sensitivity of embedded fibre optic Bragg grating sensors to disbonds in bonded composite ship joints. Compos Struct 2004;66(1–4):239–48.
[3] Li Y, Lee TH, Banu M, Hu SJ. An integrated process-performance model of ultrasonic composite welding based on finite element and artificial neural network. J Manuf Process 2020;56:1374–80.
[4] Li Y, Liu Z, Shen J, Lee TH, Banu M, Hu SJ. Weld quality prediction in ultrasonic welding of carbon fiber composite based on an ultrasonic wave transmission model. J Manuf Sci Eng 2019;141(8):081010.
[5] Sánchez-Romate XF, Sbarufatti C, Sánchez M, Bernasconi A, Scaccabarozzi D, Libonati F, et al. Fatigue crack growth identification in bonded joints by using carbon nanotube doped adhesive films. Smart Mater Struct 2020;29(3):035032.
[6] Silva-Muñoz RA, Lopez-Anido RA. Structural health monitoring of marine composite structural joints using embedded fiber Bragg grating strain sensors. Compos Struct 2009;89(2):224–34.
[7] Yu X, Fan Z, Puliyakote S, Castaings M. Remote monitoring of bond line defects between a composite panel and a stiffener using distributed piezoelectric sensors. Smart Mater Struct 2018;27(3):035014.
[8] Thoppul SD, Finegan J, Gibson RF. Mechanics of mechanically fastened joints in polymer–matrix composite structures – A review. Compos Sci Technol 2009;69(3–4):301–29.
[9] Sam-Daliri O, Faller L-M, Farahani M, Roshanghias A, Araee A, Baniassadi M, et al. Impedance analysis for condition monitoring of single lap CNT-epoxy adhesive joint. Int J Adhes Adhes 2019;88:59–65.
[10] Yousefpour A, Hojjati M, Immarigeon J-P. Fusion bonding/welding of thermoplastic composites. J Thermoplast Compos Mater 2004;17(4):303–41.
[11] Augustin T, Karsten J, Kötter B, Fiedler B. Health monitoring of scarfed CFRP joints under cyclic loading via electrical resistance measurements using carbon nanotube modified adhesive films. Compos Part A Appl Sci Manuf 2018;105:150–215.
[12] Bekas DG, Sharif-Khodaei Z, Baltzis D, Aliabadi MHF, Paipetis AS. Quality assessment and damage detection in nanomodified adhesively-bonded composite joints using inkjet-printed interdigital sensors. Compos Struct 2019;211:557–63.
[13] Bernasconi A, Kharshiduzzaman M, Comolli L. Strain Profile Measurement for Structural Health Monitoring of Woven Carbon-fiber Reinforced Polymer Composite Bonded joints by Fiber Optic Sensing Using an Optical Backscatter Reflectometer. J Adhes 2015;92(6):440–58.
[14] Deligianni A, Hale JM, Kotsikos G. Development of piezoelectric thick-film sensors to be embedded into adhesively bonded joints. Plast Rubber Compos 2016;45(4):173–80.
[15] Doshi SM, Lyness TB, Thostenson ET. Damage monitoring of adhesively bonded composite-metal hybrid joints using carbon nanotube-based sensing layer. Nanocomposites 2020;6(1):12–21.
[16] Kang M-H, Choi J-H, Kweon J-H. Fatigue life evaluation and crack detection of the adhesive joint with carbon nanotubes. Compos Struct 2014;108:417–22.
[17] Khashaba UA, Najjar IMR. Adhesive layer analysis for scarf bonded joint in CFRE composites modified with MWCNTs under tensile and fatigue loads. Compos Struct 2018;184:411–27.
[18] Kim C-H, Choi J-H, Kweon J-H. Defect detection in adhesive joints using the impedance method. Compos Struct 2015;120:183–218.
[19] Kumar S, Falzon BG, Hawkins SC. Ultrasensitive embedded sensor for composite joints based on a highly aligned carbon nanotube web. Carbon 2019;149:380–439.
[20] Mactabi R, Rosca ID, Hoa SV. Monitoring the integrity of adhesive joints during fatigue loading using carbon nanotubes. Compos Sci Technol 2013;78:1–9.
[21] Razavi SMJ, Ayatollahi MR, Nemati Giv A, Khoramishad H. Single lap joints bonded with structural adhesives reinforced with a mixture of silica nanoparticles and multi walled carbon nanotubes. Int J Adhes Adhes 2018;80:76–86.
[22] Sánchez-Romate XF, Moriche R, Pozo ÁR, Jiménez-Suárez A, Sánchez M, Güemes A, et al. Monitoring crack propagation in skin-stringer elements using carbon nanotube doped adhesive films: Influence of defects and manufacturing process. Compos Sci Technol 2020;193:108147.
[23] Sulejmani S, Sonnenfeld C, Geernaert T, Luyckx G, Mergo P, Urbanczyk W, et al. Disbond monitoring in adhesive joints using shear stress optical fiber sensors. Smart Mater Struct 2014;23(7):075006.
[24] Wong L, Chowdhury N, Wang J, Chiu WK, Kodikara J. Fatigue Damage Monitoring of a Composite Step Lap Joint Using Distributed Optical Fibre Sensors. Materials (Basel) 2016;9(5):374.
[25] Yashiro S, Wada J, Sakaida Y. A monitoring technique for disbond area in carbon fiber–reinforced polymer bonded joints using embedded fiber Bragg grating sensors: Development and experimental validation. Struct Health Monit 2017;16(2):185–201.
[26] Zeng H, Yan R, Xu L, Gui S. Application study on fiber Bragg grating sensors in damage monitoring of sandwich composite joints. J Sandw Struct Mater 2020;22(5):1542–63.
[27] Bhudolia SK, Gohel G, Fai LK, Barsotti Jr RJ. Investigation on ultrasonic welding attributes of novel carbon/Elium® composites. Materials 2020;13(5):1117.
[28] Bhudolia SK, Gohel G, Kantipudi J, Leong KF, Barsotti Jr RJ. Ultrasonic welding of novel carbon/ Elium® thermoplastic composites with flat and integrated energy directors: lap shear characterisation and fractographic investigation. Materials 2020;13(7):1634.
[29] Murray RE, Roadman J, Beach R. Fusion joining of thermoplastic composite wind turbine blades: Lap-shear bond characterization. Renew Energy 2019;140:501–12.
[30] Tsiangou E, Teixeira de Freitas S, Villegas IF, Benedictus R. Ultrasonic welding of epoxy- to polyetheretherketone- based composites: Investigation on the material of the energy director and the thickness of the coupling layer. J Compos Mater 2020;54(22):3081–98.
[31] Dubé M, Hubert P, Yousefpour A, Denault J. Resistance welding of thermoplastic composites skin/stringer joints. Compos Part A Appl Sci Manuf 2007;38(12):2541–52.

[32] Ageorges C, Ye L, Hou M. Advances in fusion bonding techniques for joining thermoplastic matrix composites: a review. Compos Part A Appl Sci Manuf 2001; 32:839–57.
[33] Brassard D, Dubé M, Tavares JR. Resistance welding of thermoplastic composites with a nanocomposite heating element. Compos B: Eng 2019;165:779–84.
[34] Brassard D, Dubé M, Tavares JR. Modelling resistance welding of thermoplastic composites with a nanocomposite heating element. J Compos Mater 2020;55(5): 625–39.
[35] Chuah YK, Chien L-H, Chang BC, Liu S-J. Effects of the shape of the energy director on far-field ultrasonic welding of thermoplastics. Polym Eng Sci 2000;40 (1):157–67.
[36] Couarraze P, Vincent G. Process development continuous induction welding of aeronautical fuselage parts-the sideffect project. In: SAMPE Europe Conference, Amsterdam, 30 September - 1 October 2020; 2020.
[37] Dubé M, Chazerain A, Hubert P, Yousefpour A, Bersee HEN. Characterization of resistance-welded thermoplastic composite double-lap joints under static and fatigue loading. J Thermoplast Compos Mater 2013;28(6):762–76.
[38] Dubé M, Hubert P, Gallet JNAH, Stavrov D, Bersee HEN, Yousefpour A. Fatigue performance characterisation of resistance-welded thermoplastic composites. Compos Sci Technol 2008;68(7–8):1759–65.
[39] Dubé M, Hubert P, Gallet JNAH, Stavrov D, Bersee HEN, Yousefpour A. Metal mesh heating element size effect in resistance welding of thermoplastic composites. J Compos Mater 2011;46(8):911–99.
[40] Endraß M, Thissen S, Jarka S, Octeau M-a, Palardy-Sim M, Robles JB, et al. Towards continuous resistance welding for full-scale aerospace components. In: SAMPE Europe Conference, Amsterdam, 30 September - 1 October 2020; 2020.
[41] Eveno EC, John W, Gillespie J. Resistance Welding of Graphite Polyetheretherketone Composites An Experimental Investigation. J Thermoplast Compos Mater 1988;1:322–38.
[42] Farahani RD, Dubé M. Novel heating elements for induction welding of carbon fiber/Polyphenylene sulfide thermoplastic composites. Adv Eng Mater 2017;19 (11):1700294.
[43] Farahani RD, Janier M, Dube M. Conductive films of silver nanoparticles as novel susceptors for induction welding of thermoplastic composites. Nanotechnology 2018;29(12):125701.
[44] Gouin O`Shaughnessey P, Dubé M, Fernandez VI. Modeling and experimental investigation of induction welding of thermoplastic composites and comparison with other welding processes. J Compos Mater 2016;50(21):2895–910.
[45] Hümbert M, Mitschang P. Characterization and modification of the temperature distribution during continuous induction welding. In: 16th European Conference on Composite Materials, Seville, 22-26 June 2014.
[46] Jongbloed B, Teuwen J, Benedictus R, Villegas IF. On differences and similarities between static and continuous ultrasonic welding of thermoplastic composites. Compos B: Eng 2020;203:108466.
[47] Jongbloed B, Teuwen JJE, Palardy G, Fernandez Villegas I. Improving weld uniformity in continuous ultrasonic welding of thermoplastic composites. In: 18th European Conference on Composite Materials, Athens, 24-28 June 2018.
[48] Ochôa P, Villegas IF, Groves RM, Benedictus R. Diagnostic of manufacturing defects in ultrasonically welded thermoplastic composite joints using ultrasonic guided waves. NDT and E Int 2019;107:102126.
[49] Palardy G, Shi H, Levy A, Le Corre S, Fernandez VI. A study on amplitude transmission in ultrasonic welding of thermoplastic composites. Compos Part A Appl Sci Manuf 2018;113:339–49.
[50] Poyraz S, Zhang L, Schroder A, Zhang X. Ultrafast Microwave Welding/ Reinforcing Approach at the Interface of Thermoplastic Materials. ACS Appl Mater Interfaces 2015;7(40):22469–77.
[51] Rohart V, Laberge Lebel L, Dubé M. Improved adhesion between stainless steel heating element and PPS polymer in resistance welding of thermoplastic composites. Compos B: Eng 2020;188:107876.
[52] Rohart V, Lebel LL, Dubé M. Influence of freeze/thaw cycling on the mechanical performance of resistance-welded carbon fibre/polyphenylene sulphide composite joints. J Reinf Plast Compos 2020;39(21–22):837–51.
[53] Rohart V, Lebel LL, Dubé M. Effects of environmental conditions on the lap shear strength of resistance-welded carbon fibre/thermoplastic composite joints. Compos B: Eng 2020;198:108239.
[54] Schieler O, Beier U, Mitschang P. Control of the through-thickness temperature distribution in carbon composite aerospace parts during induction welding. J Thermoplast Compos Mater 2017;31(12):1587–608.
[55] Senders F, van Beurden M, Palardy G, Villegas IF. Zero-flow: a novel approach to continuous ultrasonic welding of CF/PPS thermoplastic composite plates. Adv Manuf Polym Compos Sci 2016;2(3–4):83–92.
[56] Shi H, Villegas IF, Bersee HEN. Analysis of void formation in thermoplastic composites during resistance welding. J Thermoplast Compos Mater 2016;30(12): 1654–74.
[57] Shi H, Villegas IF, Octeau M-A, Bersee HEN, Yousefpour A. Continuous resistance welding of thermoplastic composites: Modelling of heat generation and heat transfer. Compos Part A Appl Sci Manuf 2015;70:16–26.
[58] Stavrov D, Bersee HEN. Resistance welding of thermoplastic composites-an overview. Compos Part A Appl Sci Manuf 2005;36(1):39–54.
[59] Sun X, Wu G, Yu J, Du C. Efficient microwave welding of polypropylene using graphite coating as primers. Mater Lett 2018;220:245–328.
[60] Talbot É, Hubert P, Dubé M, Yousefpour A. Optimization of thermoplastic composites resistance welding parameters based on transient heat transfer finite element modeling. J Thermoplast Compos Mater 2011;26(5):699–717.
[61] Tsiangou E, Teixeira de Freitas S, Fernandez Villegas I, Benedictus R. Investigation on energy director-less ultrasonic welding of polyetherimide (PEI)-to epoxy-based composites. Compos B: Eng 2019;173:107014.
[62] Villegas IF. Strength development versus process data in ultrasonic welding of thermoplastic composites with flat energy directors and its application to the definition of optimum processing parameters. Compos Part A Appl Sci Manuf 2014;65:27–37.
[63] Villegas IF, Bersee HEN. Characterisation of a metal mesh heating element for closed-loop resistance welding of thermoplastic composites. J Thermoplast Compos Mater 2015;28(1):46–65.
[64] Villegas IF, Moser L, Yousefpour A, Mitschang P, Bersee HEN. Process and performance evaluation of ultrasonic, induction and resistance welding of advanced thermoplastic composites. J Thermoplast Compos Mater 2012;26(8): 1007–24.
[65] Villegas IF, Palardy G. Ultrasonic welding of CF/PPS composites with integrated triangular energy directors: melting, flow and weld strength development. Compos Interfaces 2016;24(5):515–28.
[66] Wu T, Pan Y, Liu E, Li L. Carbon nanotube/polypropylene composite particles for microwave welding. J Appl Polym Sci 2012;126(S2):E283–9.
[67] Zhao T, Palardy G, Villegas IF, Rans C, Martinez M, Benedictus R. Mechanical behaviour of thermoplastic composites spot-welded and mechanically fastened joints: A preliminary comparison. Compos B: Eng 2017;112:224–34.
[68] Zhao T, Rans C, Fernandez Villegas I, Benedictus R. On sequential ultrasonic spot welding as an alternative to mechanical fastening in thermoplastic composite assemblies: A study on single-column multi-row single-lap shear joints. Compos Part A Appl Sci Manuf 2019;120:1–11.
[69] Yarrington P, Zhang J, Collier C. Failure Analysis of Adhesively Bonded Composite Joints. In: 46th AIAA/ASME/ASCE/AHS/ASC Structures, Structural Dynamics and Materials Conference, Austin, 18-21 April 2005; p. 2376.
[70] Augustin T, Karsten J, Fiedler B. Detection and localization of impact damages in carbon nanotube–modified epoxy adhesive films with printed circuits. Struct Health Monit 2018;17(5):1166–77.
[71] Dasilva S, Jimenez-Suarez A, Rodríguez E, Prolongo SG. Quality assessment and structural health monitoring of CNT reinforced CFRP and Ti6Al4V multi-material joints. Mater Des 2021;210:110118.
[72] Frederick H, Li W, Sands W, Tsai E, Palardy G. Multifunctional films for fusion bonding and structural health monitoring of thermoplastic composite joints. In: Society for the Advancement of Material and Process Engineering, Seattle, 4-7 May 2020.
[73] Friedrich SM, Wu AS, Thostenson ET, Chou T-W. Damage mode characterization of mechanically fastened composite joints using carbon nanotube networks. Compos Part A Appl Sci Manuf 2011;42(12):2003–209.
[74] Grammatikos SA, Kordatos EZ, Matikas TE, Paipetis AS. Real-Time Debonding Monitoring of Composite Repaired Materials via Electrical, Acoustic, and Thermographic Methods. J Mater Eng Perform 2014;23(1):169–80.
[75] Ladani RB, Wu S, Zhang J, Ghorbani K, Kinloch AJ, Mouritz AP, et al. Using Carbon Nanofibre Sensors for In-situ Detection and Monitoring of Disbonds in Bonded Composite Joints. Procedia Eng 2017;188:362–438.
[76] Li W, Frederick H, Palardy G. Multifunctional films for thermoplastic composite joints: Ultrasonic welding and damage detection under tension loading. Compos Part A Appl Sci Manuf 2021;141:106221.
[77] Li W, Palardy G. Mechanical/electrical properties of MWCNT/PP films for structural health monitoring of GF/PP joints. In: ACCE Conference, Novi, 2-4 November 2021.
[78] Lim AS, Melrose ZR, Thostenson ET, Chou T-W. Damage sensing of adhesively-bonded hybrid composite/steel joints using carbon nanotubes. Compos Sci Technol 2011;71(9):1183–2119.
[79] Park J-M, Kwon D-J, Wang Z-J, DeVries KL. Review of self-sensing of damage and interfacial evaluation using electrical resistance measurements in nano/micro carbon materials-reinforced composites. Adv Compos Mater 2015;24(3): 197–219.
[80] Sánchez-Romate XF, Moriche R, Jiménez-Suárez A, Sánchez M, Güemes A, Ureña A. An approach using highly sensitive carbon nanotube adhesive films for crack growth detection under flexural load in composite structures. Compos Struct 2019;224:111087.
[81] Thostenson ET, Chou T-W. Carbon nanotube-based health monitoring of mechanically fastened composite joints. Compos Sci Technol 2008;68(12): 2557–61.
[82] Wan Y, Hu W, Yang B, Zhao X, Xian G, Yuan Y, et al. On-line tensile damage monitoring of WGF/epoxy T-joint by the embedded MWCNT@WGF sensor. Compos Commun 2021;23:100541.
[83] Yang G, Feng X, Wang W, OuYang Q, Liu L, Wu Z. Graphene and carbon nanotube-based high-sensitive film sensors for in-situ monitoring out-of-plane shear damage of epoxy composites. Compos B: Eng 2021;204:108494.
[84] Yang X, Sun L, Huang B, Zhan B, Zhang C, Chu Y, et al. Tuning the properties of functional adhesives with hybrid nanofillers for structural health monitoring. J Adhes 2019;97(2):101–16.
[85] Zhang H, Bilotti E, Peijs T. The use of carbon nanotubes for damage sensing and structural health monitoring in laminated composites: a review. Nanocomposites 2015;1(4):167–84.
[86] Ólafsson G, Tighe RC, Boyd SW, Dulieu-Barton JM. Development of an integrated sacrificial sensor for damage detection and monitoring in composite materials and adhesively bonded joints. Struct Health Monit 2021;20(6):3406–23.
[87] Bernasconi A, Carboni M, Comolli L. Monitoring of fatigue crack growth in composite adhesively bonded joints using Fiber Bragg Gratings. Procedia Eng 2011;10:207–12.

[88] Bernasconi A, Carboni M, Comolli L, Galeazzi R, Gianneo A, Kharshiduzzaman M. Fatigue Crack Growth Monitoring in Composite Bonded Lap Joints by a Distributed Fibre Optic Sensing System and Comparison with Ultrasonic Testing. J Adhes 2016;92(7–9):739–57.
[89] Bernasconi A, Kharshiduzzaman Md, Anodio LF, Bordegoni M, Re GM, Braghin F, et al. Development of a Monitoring System for Crack Growth in Bonded Single-Lap Joints Based on the Strain Field and Visualization by Augmented Reality. J Adhes 2014;90(5–6):496–510.
[90] Canal LP, Sarfaraz R, Violakis G, Botsis J, Michaud V, Limberger HG. Monitoring strain gradients in adhesive composite joints by embedded fiber Bragg grating sensors. Compos Struct 2014;112:241–327.
[91] Capell TF, Palaniappan J, Ogin SL, Crocombe AD, Reed GT, Thorne AM, et al. The use of an embedded chirped fibre Bragg grating sensor to monitor disbond initiation and growth in adhesively bonded composite/metal single lap joints. J Opt A Pure Appl Op 2007;9(6):S40–4.
[92] Grave JHL, Håheim ML, Echtermeyer AT. Measuring changing strain fields in composites with Distributed Fiber-Optic Sensing using the optical backscatter reflectometer. Compos B: Eng 2015;74:138–46.
[93] Grundmann N, Bruning H, Tserpes K, Strohbach T, Mayer B. Influence of Embedding Fiber Optical Sensors in CFRP Film Adhesive Joints on Bond Strength. Sensors 2020;20(6):1665.
[94] Guo H, Pandher J, van Tooren M, Wang S. Process Modelling of Induction Welding for Thermoplastic Composite Materials By Neural Networks. In: SAMPE 2019, Charlotte, 20-23 May 2019.
[95] Jones R, Galea S. Health monitoring of composite repairs and joints using optical fibres. Compos Struct 2002;58(3):397–403.
[96] Karpenko O, Khomenko A, Koricho E, Haq M, Udpa L. Monitoring of fatigue damage in composite lap-joints using guided waves and FBG sensors. In: AIP Conference Proceedings, 10 February 2016; 1706: 120005.
[97] Murayama H, Kageyama K, Uzawa K, Ohara K, Igawa H. Strain monitoring of a single-lap joint with embedded fiber-optic distributed sensors. Struct Health Monit 2011;11(3):325–44.
[98] Murayama H, Ning X, Kageyama K, Wada D, Igawa H. Dynamic measurement of inside strain distributions in adhesively bonded joints by embedded fiber Bragg grating sensor. In: 23rd International Conference on Optical Fibre Sensors, Santander, 2 June 2014.
[99] Palaniappan J, Wang H, Ogin SL, Thorne A, Reed GT, Crocombe AD, et al. Structural Health Monitoring of Bonded Composite Joints Using Embedded Chirped Fibre Bragg Gratings. Adv Compos Lett 2005;14(6):185–92.
[100] Palaniappan J, Wang H, Ogin SL, Thorne AM, Reed GT, Crocombe AD, et al. Changes in the reflected spectra of embedded chirped fibre Bragg gratings used to monitor disbonding in bonded composite joints. Compos Sci Technol 2007;67(13):2847–53.
[101] Raman V, Drissi-Habti M, Limje P, Khadour A. Finer SHM-Coverage of Inter-Plies and Bondings in Smart Composite by Dual Sinusoidal Placed Distributed Optical Fiber Sensors. Sensors 2019;19(3):742.
[102] Rito RL, Crocombe AD, Ogin SL. Health monitoring of composite patch repairs using CFBG sensors: Experimental study and numerical modelling. Compos Part A Appl Sci Manuf 2017;100:255–68.
[103] Sans D, Stutz S, Renart J, Mayugo JA, Botsis J. Crack tip identification with long FBG sensors in mixed-mode delamination. Compos Struct 2012;94(9):2879–87.
[104] Shohag MA, Ndebele T, Okoli O. Real-time damage monitoring in trailing edge bondlines of wind turbine blades with triboluminescent sensors. Struct Health Monit 2019;18(4):1129–40.
[105] Wada D, Murayama H, Kageyama K, Takahashi J, Uzawa K, Igawa H. Strain distribution monitoring of CFRTP single-lap ultrasonic welding joint using embedded optical fiber sensor. In: 15th European Conference on Composite Materials, Venice, 24-28 June 2012.
[106] Webb S, Shin P, Peters K, Zikry MA, Stan N, Chadderdon S, et al. Characterization of fatigue damage in adhesively bonded lap joints through dynamic, full-spectral interrogation of fiber Bragg grating sensors: 1. Experiments Smart Mater Struct 2014;23(2):025016.
[107] Young S, Penumadu D, Foster D, Maeser H, Balijepalli B, Reese J, et al. Smart Adhesive Joint with High-Definition Fiber-Optic Sensing for Automotive Applications. Sensors 2020;20(3):614.
[108] Dugnani R, Chang F-K. Analytical model of lap-joint adhesive with embedded piezoelectric transducer for weak bond detection. J Intell Mater Syst Struct 2017;28(1):124–40.
[109] Zhuang Y, Kopsaftopoulos F, Dugnani R, Chang F-K. Integrity monitoring of adhesively bonded joints via an electromechanical impedance-based approach. Struct Health Monit 2018;17(5):1031–45.
[110] Kadlec M, Růžek R, Bělský P. Concurrent use of Z-pins for crack arrest and structural health monitoring in adhesive-bonded composite lap joints. Compos Sci Technol 2020;188:107967.
[111] Liu Q, Sun H, Wang T, Qing X. On-Site Health Monitoring of Composite Bolted Joint Using Built-In Distributed Eddy Current Sensor Network. Materials 2019;12(17):2785.
[112] Liu Q, Sun H, Chai Y, Zhu J, Wang T, Qing X. On-site monitoring of bearing failure in composite bolted joints using built-in eddy current sensing film. J Compos Mater 2021;55(14):1893–905.
[113] Andrew JJ, Arumugam V. Effect of patch hybridization on the tensile behavior of patch repaired glass/epoxy composite laminates using acoustic emission monitoring. Int J Adhes Adhes 2017;74:155–66.
[114] Andrew JJ, Arumugam V. Effect of patch hybridization on the compression behavior of patch repaired glass/epoxy composite laminates using acoustic emission monitoring. Polym Compos 2018;39(6):1922–35.
[115] Andrew JJ, Arumugam V, Bull DJ, Dhakal HN. Residual strength and damage characterization of repaired glass/epoxy composite laminates using A.E. and D.I.C. Compos Struct 2016;152:124–39.
[116] Andrew JJ, Arumugam V, Ramesh C. Acoustic emission characterization of local bending behavior for adhesively bonded hybrid external patch repaired glass/epoxy composite laminates. Struct Health Monit 2019;18(3):739–56.
[117] Bak KM, KalaiChelvan K, Vijayaraghavan GK, Sridhar BTN. Acoustic emission wavelet transform on adhesively bonded single-lap joints of composite laminate during tensile test. J Reinf Plast Compos 2013;32(2):87–95.
[118] Cao C, Dancila DS. Differentiation of Damage and Failure Mechanisms of Co-Cured Fiber-Reinforced Co-cured fiber-reinforced composite joints using acoustic emmision. J ASTM Int 2005;2(2):1–24.
[119] Saeedifar M, Saleh MN, De Freitas ST, Zarouchas D. Damage characterization of adhesively-bonded Bi-material joints using acoustic emission. Compos B: Eng 2019;176:107356.
[120] Saeedifar M, Saleh MN, Nijhuis P, de Freitas ST, Zarouchas D. Damage assessment of a titanium skin adhesively bonded to carbon fiber–reinforced plastic omega stringers using acoustic emission. Struct Health Monit 2021;21(2):407–23.
[121] Teixeira de Freitas S, Zarouchas D, Poulis JA. The use of acoustic emission and composite peel tests to detect weak adhesion in composite structures. J Adhes 2018;94(9):743–66.
[122] Vanniamparambil PA, Carmi R, Khan F, Cuadra J, Bartoli I, Kontsos A. An active–passive acoustics approach for bond-line condition monitoring in aerospace skin stiffener panels. Aerosp Sci Technol 2015;43:289–300.
[123] Xu D, Liu PF, Chen ZP, Leng JX, Jiao L. Achieving robust damage mode identification of adhesive composite joints for wind turbine blade using acoustic emission and machine learning. Compos Struct 2020;236:111840.
[124] Xu D, Liu PF, Li JG, Chen ZP. Damage mode identification of adhesive composite joints under hygrothermal environment using acoustic emission and machine learning. Compos Struct 2019;211:351–63.
[125] Zarouchas D, van Hemelrijck D. Mechanical characterization and damage assessment of thick adhesives for wind turbine blades using acoustic emission and digital image correlation techniques. J Adhes Sci Technol 2014;28(14–15):1500–16.
[126] Zhang Z, Xiao Y, Su Z, Pan Y. Continuous monitoring of tightening condition of single-lap bolted composite joints using intrinsic mode functions of acoustic emission signals: a proof-of-concept study. Struct Health Monit 2019;18(4):1219–34.
[127] Zhou W, Liu R, Lv Z-h, Chen W-y. Li X-t. Acoustic emission behaviors and damage mechanisms of adhesively bonded single-lap composite joints with adhesive defects. J Reinf Plast Compos 2015;34(1):84–92.
[128] Kupski J, Teixeira de Freitas S, Zarouchas D, Benedictus R. On the influence of overlap topology on the tensile strength of composite bonded joints: Single overlap versus overlap stacking. Int J Adhes Adhes 2020;103:102696.
[129] Caminero MA, Pavlopoulou S, Lopez-Pedrosa M, Nicolaisson BG, Pinna C, Soutis C. Analysis of adhesively bonded repairs in composites: Damage detection and prognosis. Compos Struct 2013;95:500–17.
[130] Castaings M. SH ultrasonic guided waves for the evaluation of interfacial adhesion. Ultrasonics 2014;54(7):1760–75.
[131] Coman C-D, Dima I, Hothazie S, Pelin G, Salaoru T. Temperature Effects on Damage Mechanisms of Hybrid Metal – Composite Bolted Joints Using SHM Testing Method. Incas Bulletin 2019;11(1):61–7.
[132] Haynes C, Todd M, Nadabe T, Takeda N. Monitoring of bearing failure in composite bolted connections using ultrasonic guided waves: A parametric study. Struct Health Monit 2013;13(1):94–105.
[133] Lambinet F, Khodaei ZS. Damage detection in composite skin stiffener with hybrid PZT-FO SHM system. Key Eng Mater 2017;754:367–70.
[134] Lambinet F, Sharif Khodaei Z, Aliabadi MHF. Structural Health Monitoring of Bonded Patch Repaired Composite. Key Eng Mater 2016;713:135–218.
[135] Le Crom B, Castaings M. Shear horizontal guided wave modes to infer the shear stiffness of adhesive bond layers. J Acoust Soc Am 2010;127(4):2220–30.
[136] Ma X, Bian K, Lu J-y, Xiong K. Experimental research on detection for interface debond of CFRP T-joints under tensile load. Compos Struct 2016;158:359–68.
[137] Ochôa P, Fernandez Villegas I, Groves RM, Benedictus R. Experimental assessment of the influence of welding process parameters on Lamb wave transmission across ultrasonically welded thermoplastic composite joints. Mech Syst Signal Process 2018;99:197–218.
[138] Pavlopoulou S, Grammatikos SA, Kordatos EZ, Worden K, Paipetis AS, Matikas TE, et al. Continuous debonding monitoring of a patch repaired helicopter stabilizer: Damage assessment and analysis. Compos Struct 2015;127:231–44.
[139] Quaegebeur N, Micheau P, Masson P, Castaings M. Methodology for optimal configuration in structural health monitoring of composite bonded joints. Smart Mater Struct 2012;21(10):105001.
[140] Salamone S, Fasel T, Bartoli I, Srivastava A, Scalea FL, Todd M. Health Monitoring Approach for Adhesively Bonded Joints. Mater Eval 2009;67(7):828..
[141] Sherafat MH, Guitel R, Quaegebeur N, Hubert P, Lessard L, Masson P. Structural health monitoring of a composite skin-stringer assembly using within-the-bond strategy of guided wave propagation. Mater Des 2016;90:787–94.
[142] Sherafat MH, Guitel R, Quaegebeur N, Lessard L, Hubert P, Masson P. Guided wave scattering behavior in composite bonded assemblies. Compos Struct 2016;136:696–705.
[143] Sikdar S, Ostachowicz W. Nondestructive analysis of core-junction and joint-debond effects in advanced composite structure. Polym Test 2019;73:31–8.

[144] Yang B, Xuan FZ, Xiang Y, Li D, Zhu W, Tang X, et al. Lamb Wave-Based Structural Health Monitoring on Composite Bolted Joints under Tensile Load. Materials 2017;10(6):652.
[145] Ihn J-B, Chang F-K. Detection and monitoring of hidden fatigue crack growth using a built-in piezoelectric sensor/actuator network: II. Validation using riveted joints and repair patches. Smart Mater Struct 2004;13(3):621–30.
[146] Yu X, Fan Z, Castaings M, Biateau C. Feature guided wave inspection of bond line defects between a stiffener and a composite plate. NDT and E Int 2017;89:44–55.
[147] Habib F, Martinez M, Artemev A, Brothers M. Structural health monitoring of bonded composite repairs – A critical comparison between ultrasonic Lamb wave approach and surface mounted crack sensor approach. Compos B: Eng 2013;47:26–34.
[148] Medeiros R, Souza GSC, Marques DET, Flor FR, Tita V. Vibration-based structural monitoring of bi-clamped metal-composite bonded joint: Experimental and numerical analyses. J Adhes 2020;97(10):891–917.
[149] Medeiros Rd, Borges EN, Tita V. Experimental analyses of metal-composite bonded joints damage identification. Applied Adhesion. Science 2014;2(1):1–17.
[150] Ooijevaar T, Rogge MD, Loendersloot R, Warnet L, Akkerman R, Tinga T. Vibro-acoustic modulation–based damage identification in a composite skin–stiffener structure. Struct Health Monit 2016;15(4):458–72.
[151] Ooijevaar TH, Rogge MD, Loendersloot R, Warnet LL, Akkerman R, Tinga T. Nonlinear dynamic behavior of an impact damaged composite skin–stiffener structure. J Sound Vib 2015;353:243–58.
[152] Ooijevaar TH, Warnet LL, Loendersloot R, Akkerman R, Tinga T. Impact damage identification in composite skin-stiffener structures based on modal curvatures. Structural Control and Health Monitoring 2016;23(2):198–217.
[153] Zhang Z, Xu H, Liao Y, Su Z, Xiao Y. Vibro-acoustic modulation (VAM)-inspired structural integrity monitoring and its applications to bolted composite joints. Compos Struct 2017;176:505–15.
[154] Leite Cavalcanti W, Brune K, Noeske M, Tserpes K, Ostachowicz WM, Schlag M. Adhesive Bonding Of Aircraft Composite Structures: Non-destructive Testing and Quality Assurance Concepts: Springer. Nature 2021.
[155] Ehrhart B, Ecault R, Touchard F, Boustie M, Berthe L, Bockenheimer C, et al. Development of a laser shock adhesion test for the assessment of weak adhesive bonded CFRP structures. Int J Adhes Adhes 2014;52:57–65.
[156] Ecault R, Dominguez N, Voillaume H, Campagne B, Berthe L, Boustie M, et al. Development and optimization of the laser shock wave adhesion test for composite bonding quality assessment. In: 19th World Conference on Non-Destructive Testing (WCNDT 2016), Munich, Germany, 13-17 June 2016.
[157] Ecault R, Touchard F, Boustie M, Berthe L, Dominguez N. Numerical modeling of laser-induced shock experiments for the development of the adhesion test for bonded composite materials. Compos Struct 2016;152:382–94.
[158] Gu Z, Perton M, Kruger SE, Blouin A, Lévesque D, Monchalin JP, et al. Laser Induced Shock Waves for Composites Adhesive Bond Testing. AIP Conf Proc 2010:295–302.
[159] Sagnard M, Ecault R, Touchard F, Boustie M, Berthe L. Development of the symmetrical laser shock test for weak bond inspection. Opt Laser Technol 2019;111:644–52.
[160] Fiborek P, Malinowski PH, Kudela P, Wandowski T, Ostachowicz WM. Time-domain spectral element method for modelling of the electromechanical impedance of disbonded composites. J Intell Mater Syst Struct 2018;29(16):3214–21.
[161] Malinowski P, Wandowski T, Ostachowicz W. The use of electromechanical impedance conductance signatures for detection of weak adhesive bonds of carbon fibre–reinforced polymer. Struct Health Monit 2015;14(4):332–44.
[162] Zhu J, Qing X, Liu Q, Liu X, Wang Y. Monitoring of Fiber-Reinforced Composite Single-Lap Joint with Electromechanical Impedance of Piezoelectric Transducer. Materials (Basel) 2019;12(19):3241.
[163] Almeida PD, Pereira GR. Phased array inspection of glass fiber reinforced polymers pipeline joints. J Mater Res Technol 2019;8(5):4736–40.
[164] Casavola C, Palano F, De Cillis F, Tati A, Terzi R, Luprano V. Analysis of CFRP Joints by Means of T-Pull Mechanical Test and Ultrasonic Defects Detection. Materials 2018;11(4):620.
[165] Jasiuniene E, Mazeika L, Samaitis V, Cicenas V, Mattsson D. Ultrasonic non-destructive testing of complex titanium/carbon fibre composite joints. Ultrasonics 2019;95:13–21.
[166] Mylavarapu Phani WE. Non-destructive characterization of bondlines in composite adhesive joints. J Adhes Sci Technol 2006;20(7):647–60.
[167] Taheri H, Hassen AA. Nondestructive Ultrasonic Inspection of Composite Materials: A Comparative Advantage of Phased Array Ultrasonic. Appl Sci 2019;9(8):1628.
[168] Toyama N, Yamamoto T, Urabe K, Tsuda H. Ultrasonic inspection of adhesively bonded CFRP/aluminum joints using pulsed laser scanning. Adv Compos Mater 2019;28(1):27–35.
[169] Schroeder JAAT, Chaudhry B, Shepard S. Non-destructive testing of structural composites and adhesively bonded composite joints: pulsed thermography. Compos Part A Appl Sci Manuf 2002;33(11):1511–2157.
[170] Shin PH, Webb SC, Peters KJ. Pulsed phase thermography imaging of fatigue-loaded composite adhesively bonded joints. NDT and E Int 2016;79:7–16.
[171] Tighe RC, Dulieu-Barton JM, Quinn S. Identification of kissing defects in adhesive bonds using infrared thermography. Int J Adhes Adhes 2016;64:168–78.
[172] Waugh RC, Dulieu-Barton JM, Quinn S. Pulse Phase Thermography and its Application to Kissing Defects in Adhesively Bonded Joints. Appl Mech Mater 2011;70:369–74.
[173] Kumar RLV, Bhat MR, Murthy CRL. Evaluation of kissing bond in composite adhesive lap joints using digital image correlation: Preliminary studies. Int J Adhes Adhes 2013;42:60–8.
[174] Banks WM, Dumolin F, Hayward D, Pethrick RA, Li Z-C. Non-destructive examination of composite joint structures a correlation of water absorption and high-frequency dielectric propagation. J Phys D: Appl Phys 1996;29:233–329.
[175] Tashakori S, Baghalian A, Senyurek VY, Unal M, McDaniel D, Tansel IN. Implementation of heterodyning effect for monitoring the health of adhesively bonded and fastened composite joints. Appl Ocean Res 2018;72:51–9.
[176] Pethrick RA. Non-destructive evaluation (NDE) of composites: dielectric methods for testing adhesive bonds in composites. Non-Destructive Evaluation (NDE) of Polymer Matrix Composites. Woodhead Publishing 2013:185–219.
[177] Zetina-Hernández O, Duarte-Aranda S, May-Pat A, Canché-Escamilla G, Uribe-Calderon J, Gonzalez-Chi PI, et al. Coupled electro-mechanical properties of multiwall carbon nanotube/polypropylene composites for strain sensing applications. J Mater Sci 2013;48(21):7587–93.
[178] Sánchez-Romate XF, Jiménez-Suárez A, Molinero J, Sánchez M, Güemes A, Ureña A. Development of bonded joints using novel CNT doped adhesive films: Mechanical and electrical properties. Int J Adhes Adhes 2018;86:98–104.
[179] Zhang C, Sun L, Huang B, Yang X, Chu Y, Zhan B. Electrical and mechanical properties of CNT/CB dual filler conductive adhesives (DFCAs) for automotive multi-material joints. Compos Struct 2019;225:111183.
[180] Chen J, Li H, Yu Q, Hu Y, Cui X, Zhu Y, et al. Strain sensing behaviors of stretchable conductive polymer composites loaded with different dimensional conductive fillers. Compos Sci Technol 2018;168:388–96.
[181] Ke K, Potschke P, Wiegand N, Krause B, Voit B. Tuning the Network Structure in Poly(vinylidene fluoride)/Carbon Nanotube Nanocomposites Using Carbon Black: Toward Improvements of Conductivity and Piezoresistive Sensitivity. ACS Appl Mater Interfaces 2016;8(22):14190–9.
[182] Chen J, Du X-C, Zhang W-B, Yang J-H, Zhang N, Huang T, et al. Synergistic effect of carbon nanotubes and carbon black on electrical conductivity of PA6/ABS blend. Compos Sci Technol 2013;81:1–8.
[183] Jongbloed B, Vinod R, Teuwen J, Benedictus R, Villegas IF. Improving the quality of continuous ultrasonically welded thermoplastic composite joints by adding a consolidator to the welding setup. Compos Part A Appl Sci Manuf 2022;155:106808.
[184] Köhler F, Villegas IF, Dransfeld C, Herrmann A. Static ultrasonic welding of carbon fibre unidirectional thermoplastic materials and the influence of heat generation and heat transfer. J Compos Mater 2021;55(15):2087–102.
[185] Li Y, Arinez J, Liu Z, Hwa Lee T, Fan H-T, Xiao G, et al. Ultrasonic welding of carbon fiber reinforced composite with variable blank holding force. J Manuf Sci Eng 2018;140(9):091011-1-11.
[186] Tsiangou E, Kupski J, Teixeira de Freitas S, Benedictus R, Villegas IF. On the sensitivity of ultrasonic welding of epoxy- to polyetheretherketone (PEEK)-based composites to the heating time during the welding process. Compos Part A Appl Sci Manuf 2021;144:106334.
[187] Villegas IF, Grande BV, Bersee HEN, Benedictus R. A comparative evaluation between flat and traditional energy directors for ultrasonic welding of CF/PPS thermoplastic composites. Compos Interfaces 2015;22(8):717–29.
[188] Frederick H, Li W, Palardy G. Disassembly Study of Ultrasonically Welded Thermoplastic Composite Joints via Resistance Heating. Materials 2021;14(10):2521.
[189] Li W, Palardy G. Electro-Mechanical Response of Ultrasonically Welded Thermoplastic Composite Interfaces under Static and Cyclic Flexural Loads Using Nanocomposites. ACS Applied Polymer Materials 2022;4(7):5209–23.
[190] Silva LFM, Moreira PMGP, Loureiro ALD. Determination of the strain distribution in adhesive joints using Fiber Bragg Grating (FBG). J Adhes Sci Technol 2012;28(14–15):1480–99.
[191] Dugnani R, Zhuang Y, Kopsaftopoulos F, Chang F-K. Adhesive bond-line degradation detection via a cross-correlation electromechanical impedance–based approach. Struct Health Monit 2016;15(6):650–67.
[192] Mitra M, Gopalakrishnan S. Guided wave based structural health monitoring: A review. Smart Mater Struct 2016;25(5):053001.
[193] Petrone G, Carzana A, Ricci F, De Rosa S. Damage detection through structural intensity and vibration based techniques. Advances in Aircraft and Spacecraft Science 2017;4(6):613–37.
[194] Vossen JL. Measurements of film-substrate bond strength by laser spallation: ASTM. International 1978.
[195] Ecault R, Berthe L, Touchard F, Boustie M, Lescoute E, Sollier A, et al. Experimental and numerical investigations of shock and shear wave propagation induced by femtosecond laser irradiation in epoxy resins. J Phys D: Appl Phys 2015;48(9):095501.
[196] Gay E, Berthe L, Boustie M, Arrigoni M, Trombini M. Study of the response of CFRP composite laminates to a laser-induced shock. Compos B: Eng 2014;64:108–15.
[197] Brotherhood CJ, Drinkwater BW, Dixon S. The detectability of kissing bonds in adhesive joints using ultrasonic techniques. Ultrasonics 2003;41(7):521–59.